A Simulation of a Simulation: Algorithms for Measurement-Based Quantum Computing Experiments

by

Ryohei Weil

A THESIS SUBMITTED IN PARTIAL FULFILLMENT
OF THE REQUIREMENTS FOR THE DEGREE OF

Bachelor of Science

in

THE FACULTY OF SCIENCE
(Physics and Mathematics)

The University of British Columbia
(Vancouver)

April 2022

Abstract

The paradigm of measurement-based quantum computing (MBQC) provides an ideal theoretical playground to characterize quantum computational resources. Recent advances have yielded a formalism to characterize the computational power of finite one-dimensional MBQC resource states. In this work, we develop techniques for the experimental realization of these results on Noisy Intermediate-Scale Quantum (NISQ) devices. We demonstrate a post-processing algorithm for bypassing the generally inefficient transformation to the resource states of interest. We also develop and perform a variational quantum algorithm for obtaining the coefficients of this transformation. Our results demonstrate the capability of NISQ devices for showcasing phenomena relating to computational resource characterization.

Table of Contents

List of Tables

List of Figures

List of Symbols

Quantum States

Computational basis states/ Pauli-Z eigenstates $|0\rangle, |1\rangle$

Pauli-X eigenstates $|+\rangle, |-\rangle$

Quantum Operations

All operators are represented in the computational (Pauli-Z) basis.

Quantum Wire/Identity $= I \cong \begin{bmatrix} 1 & 0 \\ 0 & 1 \end{bmatrix}$

Computational Basis Measurement 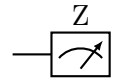 $= \Pi_0 \cong \begin{bmatrix} 1 & 0 \\ 0 & 0 \end{bmatrix}, \Pi_1 \cong \begin{bmatrix} 0 & 0 \\ 0 & 1 \end{bmatrix}$

Pauli-X (Wire) Basis Measurement 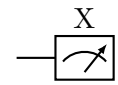 $= \Pi_0 \cong \frac{1}{2}\begin{bmatrix} 1 & 1 \\ 1 & 1 \end{bmatrix}, \Pi_1 \cong \frac{1}{2}\begin{bmatrix} 1 & -1 \\ -1 & 1 \end{bmatrix}$

Rotated Basis Measurement 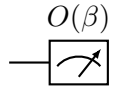 $= \Pi_0 \cong \frac{1}{2}\begin{bmatrix} 1 & e^{i\beta} \\ e^{-i\beta} & 1 \end{bmatrix}, \Pi_1 \cong \frac{1}{2}\begin{bmatrix} 1 & -e^{i\beta} \\ -e^{-i\beta} & 1 \end{bmatrix}$

Pauli-X 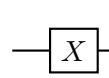 $= X \cong \begin{bmatrix} 0 & 1 \\ 1 & 0 \end{bmatrix}$

Pauli-Y 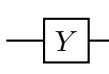 $= Y \cong \begin{bmatrix} 0 & -i \\ i & 0 \end{bmatrix}$

Pauli-Z $\quad -[Z]- = Z \cong \begin{bmatrix} 1 & 0 \\ 0 & -1 \end{bmatrix}$

X-Rotation $\quad -[R_x(\beta)]- = R_x(\beta) \cong \begin{bmatrix} \cos(\frac{\beta}{2}) & -i\sin(\frac{\beta}{2}) \\ -i\sin(\frac{\beta}{2}) & \cos(\frac{\beta}{2}) \end{bmatrix}$

Z-Rotation $\quad -[R_z(\beta)]- = R_z(\beta) \cong \begin{bmatrix} e^{-i\beta/2} & 0 \\ 0 & e^{i\beta/2} \end{bmatrix}$

Hadamard $\quad -[H]- = H \cong \frac{1}{\sqrt{2}} \begin{bmatrix} 1 & 1 \\ 1 & -1 \end{bmatrix}$

Controlled-Z $\quad$  $= CZ \cong \begin{bmatrix} 1 & 0 & 0 & 0 \\ 0 & 1 & 0 & 0 \\ 0 & 0 & 1 & 0 \\ 0 & 0 & 0 & -1 \end{bmatrix}$

Controlled-X $\quad$ 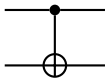 $= CX \cong \begin{bmatrix} 1 & 0 & 0 & 0 \\ 0 & 1 & 0 & 0 \\ 0 & 0 & 0 & 1 \\ 0 & 0 & 1 & 0 \end{bmatrix}$

List of Abbreviations

- CX: Controlled-X
- CZ: Controlled-Z
- MBQC: Measurement-Based Quantum Computing
- NISQ: Noisy Intermediate-Scale Quantum
- SPT: Symmetry Protected Topological
- VQE: Variational Quantum Eigensolver

Acknowledgments

I would like to thank my supervisor Robert Raussendorf for accepting me as a 449 student despite my last minute request; this project could not have been completed without his support and astute direction. I would also like my co-supervisor Arnab Adhikary for his continued mentorship and many enjoyable blackboard discussions (whether about research or TAing!). I would also like to thank the other members of the UBC Quantum Information group, and in particular Amrit Guha and Dmytro Bondarenko as fellow colleagues of the SPTMBQC experiment subgroup. Further thanks to Dmytro as well as to Elektra Dakogiannis for proofreading the thesis and for many helpful suggestions.

I acknowledge the use of IBM Quantum services for this work. The views expressed are mine, and do not reflect the official policy or position of IBM or the IBM Quantum team.

Thank you for the many friends from Science One, Physics Circle, Hugh Boyd, Choral Reef, and elsewhere that have made my undergraduate experience remarkable. Finally, thank you to my brother and my parents for their love and support through life and university.

Chapter 1

Introduction

> *And I'm not happy with all the analyses that go with just the classical theory, because nature isn't classical, dammit, and if you want to make a simulation of nature, you'd better make it quantum mechanical, and by golly it's a wonderful problem, because it doesn't look so easy.* — Richard Feynman (1981)

Though quantum simulation remains as a application of interest for quantum devices today [1], not even Feynman could have predicted the wide explosion the field of quantum computing would see in popularity and in scope. Since his 1981 keynote [2] many use cases have been discovered for quantum computers, such as in efficient prime factorization [3], database search [4], and solving linear systems of equations [5].

However, the field is arguably faced with two outstanding problems today: one experimental, and the other theoretical. Experimentally, we live in the noisy-intermediate scale quantum (NISQ) era where the available quantum devices are far too small and noisy to be able to perform most of these discovered algorithms [6]. It is not even clear that so-called quantum supremacy has been demonstrated, with the 2019 Google "demonstration" [7] being now overtaken by an improved classical algorithm [8]. On the theoretical side, the search for the property that gives quantum computers their advantage over their classical counterparts remains elusive. The intuitive condition of quantum entanglement turns out to be necessary but not sufficient, as demonstrated by the celebrated Gottesman-Knill Theorem [9] (as well as an intriguing result that most states are actually *too* entangled to be useful for quantum computation [10]).

The latter problem is interesting not only from a theoretical perspective, but also from that of application; learning of the source of quantum advantage can provide useful insights into the development of novel quantum algorithms, which has been observed to be quite difficult [11].

Fortunately, there exists a paradigm that is well-equipped to address this question; namely the scheme of measurement-based quantum computation (MBQC), as devised by Raussendorf and Briegel [12]. Unlike in the conventional circuit model of quantum computation, in MBQC the computational power is completely contained in the initial resource state, which acts as the canvas for the desired computation. Hence, characterizing such resource states can inform what are the necessary properties for universal quantum computation, and hence lead valuable insights into the nature of quantum advantage. Work on this area by Else et al. lead to a classification of resource states capable of quantum wire in 1-dimension in the language of symmetry-protected topological (SPT) phases [13]. Raussendorf et al. would then promote this classification to full one-dimensional quantum computation [14]. It was shown theoretically here that resource states away from the cluster state (the canonical MBQC resource) exhibit logical decoherence of quantum information during computation. In addition, a "divide-and-conquer" technique to manage this decoherence was introduced. While promising, this analysis was limited to infinite systems; a problem considering that any real quantum computation has to take place on a device finite in scale. To resolve this problem, recent work has given rise to a novel computational-order-parameter formalism of classifying one-dimensional resource states that applies to finite and infinite systems alike [15]. Here further results were explored and proven for the management of logical decoherence in a finite systems, which involve operations at length scales generally avoided in the infinite setting; hence titled the "counter-intuitive regime".

The work of this thesis sits at the intersection of the two defining problems above. Namely, we will demonstrate results concerning the computational power of MBQC resource states through experiment on IBM NISQ devices. We will develop and execute algorithms for performing these experiments to circumvent a major difficulty. Namely, that the known representations of the transformations used to generate the resource states of interest are non-unitary. Since quantum computers evolve states via unitary evolution, such transformations are in general not able to be implemented efficiently. Our algorithm will circumvent this difficulty by pushing the transformation past the measurement; hence allowing us to perform experiments on the easily generated cluster state and post-process accordingly to obtain the desired results. We will further develop and perform a version of a variational quantum eigensolver (VQE) algorithm that can be used to find these transformation operators using quantum devices; thus providing a fully quantum-mechanical experimental showcase of the theoretical predictions of interest. Our results will demonstrate the capability of NISQ-era devices to showcase phenomenology of MBQC resources, thus providing a step forwards to answering the questions "What are interesting things that current-era quantum computers are capable of doing?" and "How do we characterize what makes quantum computing

advantageous?"

In the proceeding chapter, we will introduce the general formalism of quantum computing in the circuit and measurement-based models. We will then discuss MBQC resource states in one dimension, introducing notions of characterizing their quantum computational power in terms of symmetry-protected topological (SPT) phases in the infinite case and the finite case. We will introduce the interpolating Hamiltonian whose ground states will be the objects of interest for experimental exploration of computational power, and a method for testing the computational power of these states through the rotation-counter rotation protocol. We end off this chapter by discussing how these ground states can be generated, as well as a general introduction to VQE algorithms. In Chapter 3, we will discuss methods of how to simulate MBQC on available circuit-based quantum computers, and in particular the algorithm to simulate the rotation-counter rotation protocol experimentally. We will also introduce the first (known) part of a VQE algorithm that can be experimentally performed to find an operator to generate the ground states of the interpolating Hamiltonian. In Chapter 4, we will theoretically derive the second half of the VQE algorithm for finding the transformation operator, and present experimental results of the rotation-counter rotation protocol for characterizing computational power of the interpolation Hamiltonian ground states. In Chapter 5 we will conclude with future directions for this work.

Chapter 2

Theory

2.1 Quantum computing 101

2.1.1 From the bit to the qubit

In the classical computing devices of today, the fundamental unit of information is the bit; a digital 0 or 1, depending on whether the value of a voltage is above some critical threshold. In quantum computers, the fundamental unit of information is instead the quantum bit, or qubit. It can be expressed as the complex superposition of the computational basis states $|0\rangle, |1\rangle$:

$$|\psi\rangle = a|0\rangle + b|1\rangle. \tag{2.1}$$

Where $|0\rangle, |1\rangle$ are the eigenstates of the Pauli-Z operator, and α, β are complex coefficients such that $|a|^2 + |b|^2 = 1$. With this normalization condition and the irrelevancy of the global phase, we may write:

$$|\psi\rangle = \cos(\theta/2)|0\rangle + e^{i\varphi}\sin(\theta/2)|1\rangle \tag{2.2}$$

which invites a useful visualization of a qubit state as a vector on the surface of the Bloch sphere, as in Fig. 2.1.

2.1.2 Qubit operations

We recall that in quantum mechanics there exist two methods of evolution; Unitary evolution and measurement. The Pauli operators are prime examples of unitary evolution, with action on

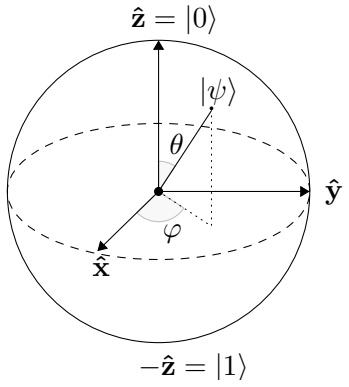

Figure 2.1: A single-qubit state $|\psi\rangle = \cos(\theta/2)|0\rangle + e^{i\phi}\sin(\theta/2)|1\rangle$ visualized on the surface of the Bloch sphere. Single-qubit unitaries can be viewed as the rotation of $|\psi\rangle$ on the sphere, and quantum measurements can be viewed as the projection of $|\psi\rangle$ onto one of two antipodal points on the sphere (e.g. $\pm\hat{\mathbf{z}} = |0/1\rangle$).

the computational basis states $X|0/1\rangle = |1/0\rangle$, $Y|0/1\rangle = \pm i|1/0\rangle$, and $Z|0/1\rangle = \pm|0/1\rangle$. These correspond to a rotation of the vector on the Bloch sphere by π radians around their respective axes. These rotations can be generalized by considering the rotation operator $R_P(\beta) = \exp(-i\beta P/2)$ (where $P \in \{X, Y, Z\}$) which corresponds to a rotation of angle β about the chosen axis. We also introduce the Hadamard operator, which is defined by the action of exchanging computational basis states with Pauli-X eigenstates: $H|0/1\rangle = |+/-\rangle = (|0\rangle \pm |1\rangle)/\sqrt{2}$ and $H|+/-\rangle = |0/1\rangle$ (note this also implies that $HZH = X$; something we will make use of later on). In general, all single-qubit unitaries can be viewed as rotations about the Bloch sphere, as visualized in Fig. 2.2.

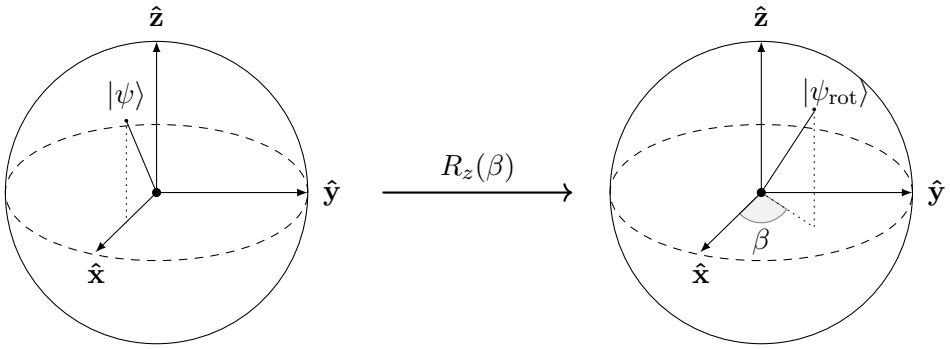

Figure 2.2: Bloch sphere visualization of single-qubit unitaries. Here the unitary $R_z(\beta)$ is applied to the state $|\psi\rangle$, rotating the state by angle β about the z-axis of the Bloch sphere.

We also consider multi-qubit unitaries, which are necessary operations to entangle qubits. First, we recall the tensor product formalism of composing multiple quantum systems; for example, the system of two qubits in the $|0\rangle$ states is written as $|0\rangle \otimes |0\rangle$ or abbreviated as $|00\rangle$ or $|0\rangle^{\otimes 2}$. We can then define operations that act on these multi-qubit quantum states. For example, the controlled-X gate acts on the basis states as $CX_{12}|00\rangle = |00\rangle, CX_{12}|01\rangle = |01\rangle, CX_{12}|10\rangle = |11\rangle$, and $CX_{12}|11\rangle = |10\rangle$. Given an (unentangled) input state of $|+0\rangle$ the $CX_{1,2}$ gate will produce the (entangled) bell state:

$$CX_{12}|+0\rangle = \frac{CX_{12}|00\rangle + CX_{12}|10\rangle}{\sqrt{2}} = \frac{|00\rangle + |11\rangle}{\sqrt{2}} =: |B_{00}\rangle \tag{2.3}$$

For measurements, we consider some Hermitian observable $O = \sum_i \lambda_i |\phi_i\rangle\langle\phi_i|$ where λ_i are the (real) eigenvalues and $|\phi_i\rangle$ the eigenstates. For non-degenerate observables, the post-measurement outcomes are given by the eigenstates $|\phi_i\rangle$ (where λ_i is the measured outcome) and the measurement probabilities by $p(i) = |\langle\phi_i|\psi\rangle|^2$. In terms of the Bloch sphere picture, measurements can be viewed as collapsing the state $|\psi\rangle$ onto one of two antipodal points corresponding to the eigenstates of the measured observable (for example the north and south poles for the computational basis states $|0\rangle$ and $|1\rangle$, as in Fig. 2.3).

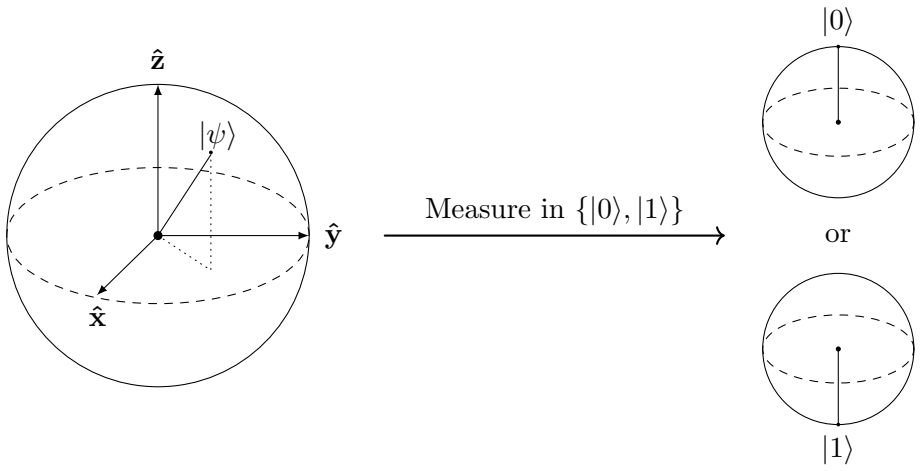

Figure 2.3: Bloch sphere visualization of qubit measurement. Here the state $|\psi\rangle$ is measured in the computational basis $\{|0\rangle, |1\rangle\}$. The post-measurement states are antipodal points on the Bloch sphere, with probability $p(0) = |\langle 0|\psi\rangle|^2$ of obtaining $|0\rangle$ and $p(1) = |\langle 1|\psi\rangle|^2$ of obtaining $|1\rangle$.

2.1.3 The circuit model

The Circuit Model is the standard paradigm of quantum computation. It operates in analogy to the circuit model of classical computation, where one starts with a register of bits initialized in the 0 state and proceeds with the computation by the application of logic gates (such as `AND` and `NOT`). In a quantum circuit, one starts with a register of qubits in the $|0\rangle$ states, and then evolves the state through a computation-specific sequence of unitary quantum gates. At the end of the computation, all qubits are measured in the computational basis as a readout procedure. The computation is in general repeated many times to account for the probabilistic nature of the final measurement.

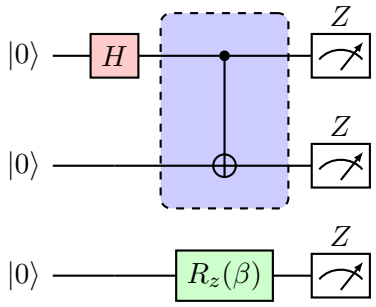

Figure 2.4: A 3-qubit example of a quantum circuit. The computation begins with a register of qubits in the $|0\rangle^{\otimes 3}$ state. The computation proceeds by the application of unitary quantum gates, such as single-qubit gates like the Hadamard gate (red) and $R_z(\beta)$ rotation gate (green) as well as entangling gates such as the CX gate (blue). The qubits are all measured in the computational basis $\{|0\rangle, |1\rangle\}$ in the end to obtain the information stored in the state.

Much like the `NAND` gate forms a universal gate set in classical computation (where one can emulate any other logic gate through use of `NAND` gates alone) [16], a similar notion exists in quantum computing. Namely, a set of quantum gates is labelled as universal if a the composition of gates from the set can form any unitary transformation up to an arbitrarily small error. Although there are more restrictive gate sets, the set composed of single-qubit rotations and the CX gate is quantum computationally universal [17]. Therefore, if any other computational model is able to emulate these two types of operations and their composition, it can be labelled as universal.

2.2 Measurement-based quantum computing (MBQC) in 1D

2.2.1 Motivating MBQC

Although the circuit model is the dominant paradigm of quantum computing (and most physical realizations of quantum computers today, such as by Google and IBM invoke this model), this paradigm is ill-suited to address the question of where quantum computers obtain their advantage. Currently, quantum algorithms such as Shor's algorithm for prime factorization [3] seem to suggest that quantum computers possess some kind of theoretical advantage over their classical counterparts. However, the source of this advantage remains a open problem. Quantum mechanical properties such as superposition and entanglement turn out to be necessary but not sufficient conditions for such advantage.

One can, for example, have a local n-qubit state of the form $|\Psi\rangle = |\psi\rangle_1 \otimes |\psi\rangle_2 \otimes \ldots \otimes |\psi\rangle_n$ that is in superposition, but the locality of the state means that it can be efficiently simulated with $O(n)$ coefficients (which can be easily simulated classically). In addition, while a general entangled quantum state and its evolution requires an exponential number of coefficients to simulate classically (with $O(2^n)$ coefficients required to specify a general entangled n-qubit quantum state) but the celebrated Gottesman-Knill theorem [9] shows that quantum computation that proceeds via gates only from the Clifford group (that includes entangling gates such as CX) can be simulated in polynomial time. In a twist, there are actually results that show that most quantum states are actually "too entangled" for use in quantum computation [10]!

The circuit model is not optimal for characterization of quantum advantage given that the gates used are highly computation dependent and the computational power of gates is made unclear by results such as the Gottesman-Knill theorem. We therefore desire a model which is computationally equivalent but for which this analysis is easier. We therefore consider the paradigm of measurement-based quantum computation, as introduced by Raussendorf and Briegel [12]. In this model, computation begins by preparing qubits into an initial state, known as a "resource state". The computation then proceeds by adaptive single-qubit measurements on the resource state, with the sequence of single-qubit measurements simulating the computation as it would have been carried out in the circuit model. The benefit of the MBQC model is that the resource state used is independent of the choice of computation, being a universal canvas on which the computation can be etched out by measurements. Therefore, in this picture characterization of quantum computational advantage becomes a question of characterizing such resource states.

In this section, we will start by defining the cluster state, which is the canonical MBQC re-

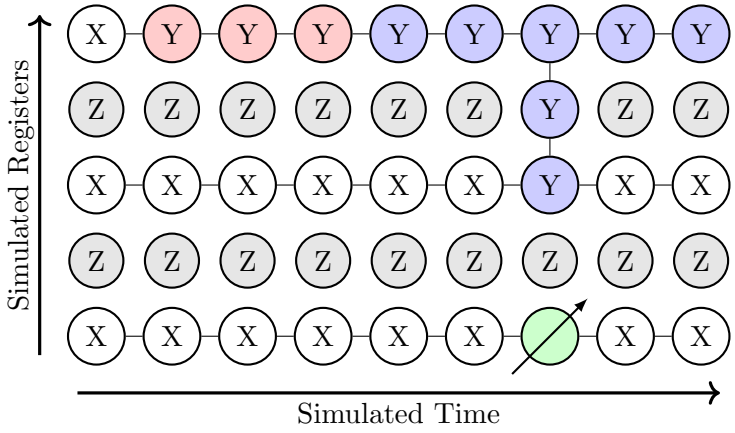

Figure 2.5: Example of quantum computation in the measurement-based formalism, simulating the circuit computation in Fig. 2.4. Computation proceeds by single-qubit measurements on an initial resource state. Here the resource state is two dimensional, with one dimension acting as the simulated qubit registers, and one dimension acting as simulated time. The qubit measurements in X simulate quantum wire, qubit measurements in red simulate the Hadamard gate, the qubit measurements in blue simulate the CX gate, and the measurement in green simulates the $R_z(\beta)$ gate.

source state. We will then study operations on the cluster state in 1-dimension to show how the measurement-based model can simulate the evolution of a single qubit. As the central topic of the thesis concerns one-dimensional MBQC resources, we will omit a full universality proof of the MBQC model, which requires discussion of 2-dimensional resource states and operations.

2.2.2 The cluster state

We here provide two equivalent definitions of the cluster state in one dimension. The first is an operational definition, and will be useful for when we require the creation of cluster states on quantum devices.

Definition (Cluster Chain). The cluster chain $|C\rangle$ is the quantum state obtained via the following procedure:

1. Start with a register/chain of n qubits each initialized to $|0\rangle$: $|0\rangle^{\otimes n}$.
2. Apply Hadamard gates to each qubit to obtain $|+\rangle^{\otimes n}$.
3. Apply controlled-Z gates between neighbouring qubits in the chain to obtain the cluster state $|C\rangle$.

Note that the entanglement generated in step 3 of the above procedure can be equivalently implemented via an translation-invariant Ising interaction for a fixed amount of time (independent of the system size). An equivalent definition of the state involves Hamiltonians:

Definition (Cluster Chain). The cluster chain $|C\rangle$ is the unique ground state of the Hamiltonian $H_c = -\sum_i Z_{i-1}X_iZ_{i+1}$. Alternatively, it is the unique quantum state for which $Z_{i-1}X_iZ_{i+1}|C\rangle = +|C\rangle$ for each site i. Therein, the set of $Z_{i-1}X_iZ_{i+1}$ operators generates the stabilizer group of the cluster state.

While the first definition will help us to demonstrate the mechanism of MBQC in one-dimension, the second will be extremely useful when we enter discussion of generalized one-dimensional resource states.

2.2.3 Operating on the cluster state

Having now established what the cluster state is, we discuss how one can carry out MBQC on this state. We will demonstrate three capabilities; quantum wire (the identity operation), z-rotations, x-rotations, and general rotations. Much of the development in this section is modelled after the discussion in [15].

Quantum wire

We consider a 2-qubit cluster state where the first qubit is some input state $|\psi_{in}\rangle = \alpha|0\rangle + \beta|1\rangle$. So, our starting state is $|\Psi\rangle = CZ_{12}(|\psi_{in}\rangle \otimes |+\rangle)$. We wish to find a way to move the input state from the first qubit to the second without modifying it (i.e. perform a wire operation). To this end, we consider measuring the first qubit in the Pauli-X eigenbasis of $\{|+\rangle, |-\rangle\}$. Expanding out the first qubit in this basis, we find:

$$\begin{aligned}
|\Psi\rangle &= CZ_{12}((\alpha|0\rangle + \beta|1\rangle) \otimes |+\rangle) \\
&= \alpha|0\rangle|+\rangle + \beta|1\rangle|-\rangle \\
&= \alpha\left(\frac{|+\rangle + |-\rangle}{\sqrt{2}}\right)|+\rangle + \beta\left(\frac{|+\rangle - |-\rangle}{\sqrt{2}}\right)|-\rangle \\
&= |+\rangle\left(\frac{\alpha}{\sqrt{2}}|+\rangle + \frac{\beta}{\sqrt{2}}|-\rangle\right) + |-\rangle\left(\frac{\alpha}{\sqrt{2}}|+\rangle - \frac{\beta}{\sqrt{2}}|-\rangle\right) \\
&= \frac{1}{\sqrt{2}}\left(|+\rangle H|\psi_{in}\rangle + |-\rangle HZ|\psi_{in}\rangle\right)
\end{aligned}$$

So after the measurement of the first qubit, the post-measurement state of the second qubit is:

$$|\psi_{out}\rangle = HZ^s|\psi_{in}\rangle$$

where $s = 0$ or 1 depending on whether the measurement on the first qubit yields the positive or negative eigenvalue respectively. Graphically, we can picture this as the circuit identity in Fig. 2.6.

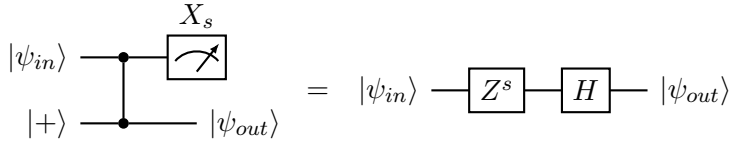

Figure 2.6: Quantum half-teleportation circuit identity.

The above protocol can be recognized as a variant of the famous quantum teleportation protocol [18], with the modification that we measure in a single-qubit basis (rather than the Bell basis) and only require one classical bit of information (s) to post-process the result (compared to two). Thus, we have demonstrated that we can perform quantum wire/the identity operation on the cluster state through measurement alone.

z-rotations

While the ability to do nothing is certainly appreciated, we certainly want to be able to do more than just shuttle our state down our cluster chain. As a first step, we consider how we might carry out z-rotations on our input state. Of course, in the circuit model this would be as simple as just applying the $R_z(\beta)$ gate to our initial state. However, we don't have access to such gates! So we are tasked with finding a way to implement this rotation through measurement alone. To this end, we consider a quantum circuit that applies some unitary operator U followed by a measurement in the eigenbasis of an observable O. We can write the projectors corresponding to the measurement

as $\Pi_{O,\pm} = \frac{I \pm O}{2}$ where I is the identity gate. The action of this circuit is then:

$$\begin{aligned}
\Pi_{O,\pm} U &= U U^\dagger \frac{I \pm O}{2} U \\
&= U \frac{U^\dagger I U + U^\dagger O U}{2} \\
&= U \frac{I + U^\dagger O U}{2} \\
&= U \Pi_{U^\dagger O U, \pm}
\end{aligned}$$

where we use that $U^\dagger U = I$ for unitary operators. We conclude that:

$$\Pi_{O,\pm} U = U \Pi_{U^\dagger O U, \pm} \tag{2.4}$$

The above manipulations tell us that applying a unitary operator U and then measuring in O is totally equivalent to skipping the unitary and just measuring the new observable $U^\dagger O U$ Note we can discard the U in front of the projector in the last line as we don't particularly care about what happens after measurement. With this in mind, we now consider the circuit identity in Figure. 2.7.

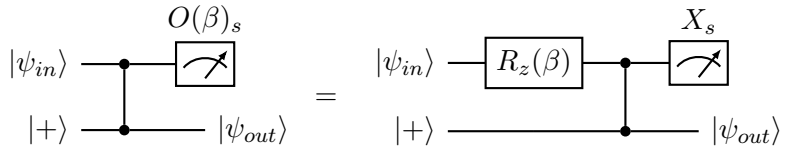

Figure 2.7: z-rotation circuit identity.

where we have commuted the $R_z(\beta)$ past the CZ gate and then applied the unitary-projector identity as derived above. We now measure the first qubit in the eigenbasis of the observable:

$$O(\beta) = R_z(\beta)^\dagger X R_z(\beta) = \cos(\beta) X - \sin(\beta) Y.$$

So combining this identity with the quantum wire result, the output on the second qubit of this circuit is:

$$|\psi_{out}\rangle = H Z^s R_z(\beta) |\psi_{in}\rangle$$

Let us recap what we have done here. We wanted to find a way to not just teleport but also rotate our input qubit. In the circuit model, we could just apply a z-rotation gate, but now we want to

accomplish this with measurements alone. So, we derived a unitary-projector identity and showed that the action of a z-rotation unitary gate is equivalent to just changing our measurement basis to $O(\beta) = R_z(\beta)^\dagger X R_z(\beta)$. Combining this with the quantum wire result, we have now derived a way to apply a rotation to our simulated qubit through measurements alone.

x-rotations

We've now found ways to perform the identity operation, and to rotate in z; but of course there are more rotations possible than just that! We now wish to find a method to rotate about the x-axis. To this end, we consider a similar setup to the above z-rotation argument, but now on a cluster state of three qubits instead of two (with again an input state $|\psi_{in}\rangle$ on the first qubit). Suppose we measure the first qubit in the wire (X) basis with outcome s_1 and measure the second qubit in the rotated basis $O(\beta)$ with outcome s_2. Combining the results of the previous two sections, the output state will be:

$$\begin{aligned}
|\psi_{out}\rangle &= (HZ^{s_2}R_z(\beta))(HZ^{s_1})|\psi_{in}\rangle \\
&= (HZ^{s_2}R_z(\beta)H)Z^{s_1}|\psi_{in}\rangle \\
&= X^{s_2}R_x(\beta)Z^{s_1}|\psi_{in}\rangle \\
&= X^{s_2}Z^{s_1}R_x((-1)^{s_1}\beta)|\psi_{in}\rangle
\end{aligned}$$

Where in the third line we make use of the Hadamard conjugation identity of $HZH = X$ and in the fourth line we use that $ZX = -XZ$.

This almost looks like the x-rotation that we want! As before, we note the presence of operators sitting in front of the state. These are so-called "byproduct operators" in MBQC, which are dependent on the probabilistic measurement outcomes. We can keep track of these operators throughout the computation and account for them at the end, so they do not pose a significant problem. More concerning is the presence of the $(-1)^{s_1}$ in the x-rotation. It seems as though depending on the measurement outcome on the first qubit, we have a 50/50 chance of rotating our state by a positive or negative angle, and hence our operation seems to be probabilistic! However this is not the case. What the above expression really tells us is that depending on the outcome s_1 of our first measurement, we should adjust the measurement basis of our second measurement to be $O((-1)^{s_1}\beta)$ accordingly so as to perform the correct (positive) rotation that we desire. Note that this enforces a *temporal order* of measurements, as future measurements are adaptive based

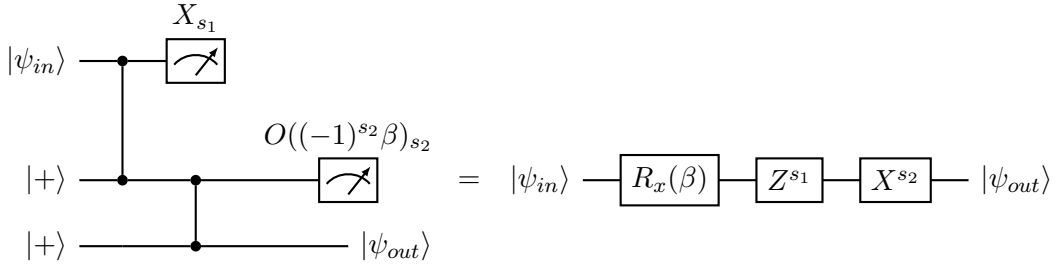

Figure 2.8: x-rotation circuit identity.

on outcomes of the past. With this adaptive measurement, we obtain the post measurement state:

$$\begin{aligned}|\psi_{out}\rangle &= (HZ^{s_2}R_z((-1)^{s_1}\beta))(HZ^{s_1})|\psi_{in}\rangle \\ &= X^{s_2}Z^{s_1}R_x(\beta)|\psi_{in}\rangle\end{aligned}$$

which is the desired x-rotation performed on our state! In all, this yields the circuit identity depicted in Fig. 2.8.

There are three takeaways here. The first is that we have managed to accomplish a x-rotation via measurements on the cluster state. The second is that in MBQC there are byproduct operators which are harmless, but have to be kept track of as the computation proceeds in order to account for them on the output. Finally, in order to induce the correct state evolution, we require adaptively changing our measurement bases based on past measurement outcomes; hence MBQC has a temporal order.

General rotations

We are extremely close to our desired end goal of performing arbitrary rotations through measurement on a 1-dimensional cluster chain. The final piece of our puzzle is provided by the great late Euler, who informs us that any rotation U can be decomposed as:

$$U = R_x(\gamma)R_z(\beta)R_x(\alpha)$$

for some $\alpha, \beta, \gamma \in \mathbb{R}$. To accomplish this, we extend our earlier argument to a five qubit cluster state with input $|\psi_{in}\rangle$. We measure the first qubit in the wire (X) basis, and perform measurements on the second/third/fourth qubits in the rotated bases $O(\phi_2), O(\phi_3), O(\phi_4)$ with ϕ_i chosen to perform

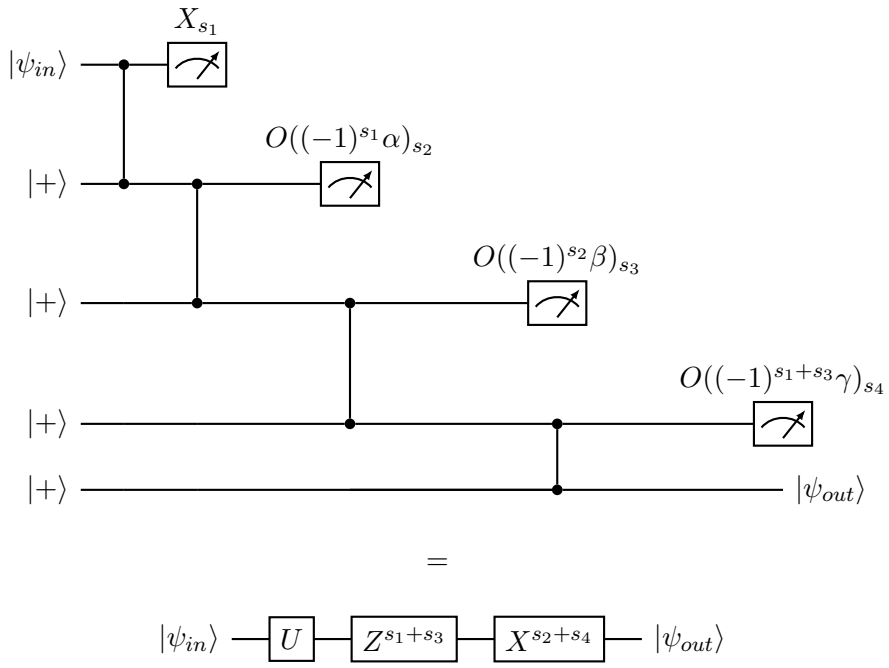

Figure 2.9: Circuit identity for general rotations.

U. From the results of the previous sections, the output state will be:

$$\begin{aligned}
|\psi_{out}\rangle &= (HZ^{s_4}R_z(\phi_4))(HZ^{s_3}R_z(\phi_3))(HZ^{s_2}R_z(\phi_2))HZ^{s_1}|\psi_{in}\rangle \\
&= [HZ^{s_4}R_z(\phi_4)H]Z^{s_3}R_z(\phi_3)[HZ^{s_2}R_z(\phi_2)H]Z^{s_1}|\psi_{in}\rangle \\
&= X^{s_4}R_x(\phi_4)Z^{s_3}R_z(\phi_3)X^{s_2}R_x(\phi_2)Z^{s_1}|\psi_{in}\rangle \\
&= X^{s_2+s_4}Z^{s_1+s_3}R_x((-1)^{s_1+s_3}\phi_4)R_z((-1)^{s_2}\phi_3)R_x((-1)^{s_1}\phi_2)|\psi_{in}\rangle
\end{aligned}$$

So adaptively choosing $\phi_2 = (-1)^{s_1}\alpha$, $\phi_3 = (-1)^{s_2}\beta$, and $\phi_4 = (-1)^{s_1+s_3}\gamma$ based on measurement outcomes, we obtain output:

$$\begin{aligned}
|\psi_{out}\rangle &= X^{s_2+s_4}Z^{s_1+s_3}R_x(\gamma)R_z(\beta)R_x(\alpha)|\psi_{in}\rangle \\
&= X^{s_2+s_4}Z^{s_1+s_3}U|\psi_{in}\rangle
\end{aligned}$$

and we have therefore accomplished our arbitrary rotation (up to byproduct operators)!

We have therefore shown that the cluster state is capable of performing arbitrary rotations/single-

qubit unitaries on a single logical/simulated qubit, through use of adaptive measurements and some classical side-processing only; thus MBQC is equivalent computationally to a single qubit in the circuit model! A full universality proof would require going into the realm of two-dimensional cluster states, where we could then discuss the simulation of multiple qubits and entangling gates between them. However, we refer readers to sources such as [12] for full universality proofs as two-dimensional cluster states largely lie outside the scope of this thesis.

2.2.4 Computational power

To conclude this section, we introduce an operational definition of computational power of states:

Definition (Computational power). The computational power of a one-dimensional quantum state is defined as its ability to carry out MBQC; that is, perform quantum wire and arbitrary single-qubit unitaries.

From the above analysis, we would conclude that the cluster state has full computational power. As a foil to the cluster state, we also introduce the product state $|+\rangle^{\otimes n}$, which is the ground state of the local magnetic field Hamiltonian $H_p = -\sum_i X_i$. Given the fact that the product state is unentangled, it possesses no capability to perform MBQC. Intuitively, no operations on one part of the state can affect the other, and measurements on one part of the state just destroy the information contained in that part of the state. We will soon return to discussion of the cluster and product state when we introduce the interpolation Hamiltonian.

2.3 MBQC resources in 1D

In the previous section, we introduced the 1-dimensional cluster state, and demonstrated how an adaptive measurement sequence on this state could simulate any single-qubit unitary. However, one may now wonder if the cluster state is the unique state for which such a measurement-based computation protocol is possible. This turns out to be *not* the case, and such a property turns out to be a property of an entire phase of matter, rather than a particular special state (such as the cluster state). In this section, we will give a non-technical overview of computational phases of matter and how symmetry can characterize resource states in one-dimension. We will then discuss a recent development for characterizing the computational power of *finite* MBQC resource states, where the notion of phases becomes ill-defined.

2.3.1 SPT order and computational power

Classically, a thermodynamic phase of a system is a region of phase space for which properties of materials are uniform. Phase transitions are characterized under the Ehrenfest classification by non-differentiability in thermodynamic state functions (such as free energy) as parameters (such as temperature) are varied as we pass through the transition. Going from the realm of classical to quantum, quantum phases are defined at zero temperature; if we are interested in studying phase transitions due to quantum fluctuations, we must remove thermal fluctuations that could wash out the quantum ones. At zero temperature, the systems of interest must be in the ground state and therefore quantum phases are characterized by the ground state of systems and the energy gap between the ground state and first excited state [19].

For many decades, the Landau's symmetry-breaking theory of phase transitions [20] was thought to be capable of describing all possible phase transitions; in this formalism the Hamiltonian possesses more symmetry than the ground states (leading to the title of "symmetry-breaking"). However, discoveries such as fractional quantum Hall states that inherit the symmetry of the Hamiltonian [21] paved the way for the new formalism, namely that of topological order [22]. First, we introduce the notion of a gapped quantum phase, where gapped refers to the fact that the energy gap between the ground state and first excited state of the Hamiltonians of interest do not vanish in the thermodynamic limit:

Definition (Gapped Quantum Phase). *Two gapped states $|\psi_0\rangle, |\psi_1\rangle$ belong in distinct gapped quantum phases if Hamiltonians H_0, H_1 which they are ground states of can be smoothly deformed into each other without closing the gap. Equivalently, they belong in the same phase if and only if they are related by a local (system size-independent) unitary transformation.*

From this follows the definition of topological order:

Definition (Topological Order). *A gapped state $|\psi_0\rangle$ possesses non-trivial topological order if the Hamiltonian it is the ground state of cannot be smoothly connected to the product state Hamiltonian without closing the gap. Equivalently, there exists no local unitary transformation that connects $|\psi_0\rangle$ to the product phase.*

However, the above notion of topological order makes no reference to the concept of symmetries associated with the problem. Inclusion of these symmetries can lead to interesting classifications, motivating the definition of symmetry-protected topological (SPT) order:

Definition (Symmetry-Protected Topological Order). *States $|\psi_0\rangle$, $|\psi_1\rangle$ with a given symmetry belong in distinct SPT phases if they cannot be smoothly deformed into each other via a low-depth local unitary circuit (that is, a circuit whose depth which does not scale with the system*

size) that respects the symmetry. A state belongs to a non-trivial SPT phase if it cannot be connected via a symmetry-respecting low-depth local unitary circuit to the product state.

How does all of this condensed-matter theoretic discussion of phases connect back to our discussion of quantum computation? The breakthrough connection between SPTO and computational power was first made by Else et al., who showed that the ability for a state to carry out quantum wire was a consequence of the symmetry-protected phase [13]. Raussendorf et al. would generalize this notion to show that computational power as a whole is uniform across each symmetry-protected topologically ordered phase [14]. In particular, the cluster state lives in a symmetry-protected phase with a $\mathbb{Z}_2 \times \mathbb{Z}_2$ symmetry (where the symmetry group is generated by $IXIXIX\ldots$ and $XIXIXI\ldots$), and the computational power of states that live in this SPT phase are uniform.

The takeaways here are twofold. First, the characterization of computational power in terms of symmetry further elucidates the question of the source of quantum computational advantage, as the capability to do quantum computation has now reduced to a question of a classification of symmetries. Second, computational power is in some sense a robust property. Rather than being a property of specific states (e.g. the cluster state), it belongs an entire symmetry-protected phase of matter. This is useful in the sense that preparing states exactly experimentally may be difficult due to real-world noise, but slight perturbations to useful states (that do not take them outside of the computationally useful phase) are still computationally powerful. This second takeaway ties into the main objective of the thesis, namely, can we demonstrate this robustness experimentally?

2.3.2 The interpolating Hamiltonian

In this section, we concretely discuss one-dimensional computational phases, and introduce a Hamiltonian that will play a central role to the thesis. To this end, we recall the definition of the cluster state $|C\rangle$ as the ground state of the Hamiltonian $H_c = -\sum_i Z_{i-1}X_iZ_{i+1}$ and the definition of the product state $|+\rangle^{\otimes n}$ as the ground state of the Hamiltonian $H_p = -\sum_i X_i$. We then consider the interpolation Hamiltonian, defined as:

$$H(\alpha) \cong -\cos(\alpha)\sum_i Z_{i-1}X_iZ_{i+1} - \sin(\alpha)\sum_i X_i \tag{2.5}$$

The ground states $|\phi(\alpha)\rangle$ of this Hamiltonian all lie in the trivial topological phase as we can vary α smoothly to get to $H(\frac{\pi}{2}) = -\sin(\frac{\pi}{2})\sum_i X_i = H_p$; i.e. we can connect the Hamiltonians smoothly without closing the gap. However, there are two distinct symmetry-protected topological phases that arise from this Hamiltonian. The Hamiltonian possesses a $\mathbb{Z}_2 \otimes \mathbb{Z}_2$ symmetry that the ground

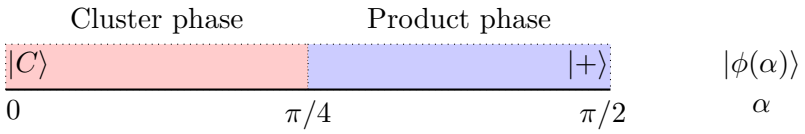

Figure 2.10: Phase diagram for ground states of interpolating Hamiltonian $H(\alpha)$. For $\alpha < \frac{\pi}{4}$, the states reside in the computationally useful cluster phase. For $\alpha > \frac{\pi}{4}$, the states reside in the computationally useless product phase.

states inherit. In the thermodynamic limit, there is no way to connect the Hamiltonians with $\alpha < \frac{\pi}{4}$ to the Hamiltonians for $\alpha > \frac{\pi}{4}$ via a path that respects the symmetry that does not close the gap above the ground state. Equivalently, there is no local low-depth unitary circuit that smoothly connects the ground states of $\alpha < \frac{\pi}{4}$ to $\alpha > \frac{\pi}{4}$ via a path that respects the symmetry. We therefore denote the states for $\alpha < \frac{\pi}{4}$ as residing in the cluster phase and the states for $\alpha > \frac{\pi}{4}$ as residing in the product phase. The work of [14] proved the uniformity of computational power of states in these phases, proving that states in the cluster phase are equivalently powerful in MBQC as the cluster state and states in the product phase as useless as the product state.

2.3.3 Characterizing finite resources

It would seem as if the formalism of symmetry-protected topological phases puts a nice bow on the problem of characterizing quantum computational resources[1]; this is unfortunately not the case. While the problem is resolved in the thermodynamic limit, an infinitely large quantum computer cannot physically exist, with any real quantum computation takes place in a finite setting. This is further exacerbated by the current landscape of quantum computing, where available devices are still quite small (on the order of 10s of qubits). The notion of a computational phase becomes ill-defined in such finite settings. As a prime example, we consider again the Hamiltonian given by (2.5). Looking at the ground states of such Hamiltonians for finite spin chains, we find that the gap *never* closes when a symmetry-respecting path is taken [15]. Hence all ground states in the finite regime belong to the same phase. However, we still have the sense in the finite setting that $|C\rangle = |\phi(0)\rangle$ and $|+\rangle^{\otimes n} = |\phi(\pi/2)\rangle$ have strikingly different computational capabilities, and intuitively we feel as though states "close" to the cluster state should have more power than states close to the product state.

The results in [15] provide the resolution for the finite regime. Namely, Adhikary reveals the connection between computational order parameters with string order parameters used in

[1] or at least, in one dimension

condensed matter physics to distinguish between SPT phases. In this formalism (which we note applies equally as well to finite and infinite systems to characterize computational power), the computational power of the ground states of $H(\alpha)$ for a odd length n chain can be characterized by the expectation value:

$$2\nu_{01}(\alpha) = \langle\phi(\alpha)|Z_k X_{k+1} I_{k+2} X_{k+3} \dots I_{n-2} X_{n-1} Z_n|\phi(\alpha)\rangle \tag{2.6}$$

2.3.4 Decoherence, division, and correlation length

Thus far we have glossed over what happens when one tries to do MBQC with ground states of (2.5) that are away from the cluster state. In fact, it would be reasonable to meet the result of [14] and the display of computational power in Fig. 2.10 with confusion; how are ground states $|\phi(\alpha)\rangle$ of $H(\alpha)$ for $0 < \alpha < \frac{\pi}{4}$ equally as powerful as the cluster state, when in going away from cluster state we are adding "computational uselessness" in the form of the product state term?

The devil lies in the details; as one does MBQC on states away from the cluster state, one finds that symmetry breaking measurements generate decoherence. The formal reason for this is that symmetry-respecting (i.e. X-basis if we recall the $\mathbb{Z}_2 \otimes \mathbb{Z}_2$ symmetry of $H(\alpha)$) measurements prevent the mixing of the so-called logical and junk subsystems but symmetry-breaking measurements (i.e. rotations) which are necessary to carry out one-dimensional computation entangles these two systems, leading to the loss of quantum information [13].

At this point, the skeptical reader may object that it doesn't sound as though computational power should be uniform within the cluster phase at all, if symmetry breaking measurements on non-cluster states results in loss of information! Therein, we present (but do not prove) the result from [14] that within the cluster phase, one can use the construction of "oblivious wire" to implement rotations in the cluster phase with error quadratic in the measurement angle. This immediately presents a way to reduce the decoherence attained through rotations; namely by splitting of the rotation angle. If we have that the error is $\epsilon(\beta) \propto O(\beta^2)$, then the effect of splitting the measurement into N smaller rotations is therefore:

$$\epsilon(\beta_{\text{split}}) = NO((\beta/N)^2) = O(\beta^2/N)$$

so the takeaway is that in the infinite setting we can chop up our rotation as finely as we like (take N large) for states within the cluster phase to decrease our error arbitrarily, in a technique known as "divide-and-conquer". With this technique, states in the cluster phase can be said to have uniform computational power.

Now moving back to the finite setting, the idea of "chopping up the rotation as finely as we like" is no doubt setting off alarm bells as of course this was a luxury only affordable to us when we had infinite number of qubits to work with. In fact the problem is even more complex; there is a α-dependent correlation length of the system $\xi(\alpha)$. In the infinite setting, the textbook approach is to take the distance Δ between successive rotations to be $\Delta \gg \xi(\alpha)$ such that the rotations can be considered independently. In the finite setting then, there appears to be a trade-off. Does one split the rotation finely so as to minimize the decoherence from rotations but where $\Delta \approx \eta(\alpha)$ leads to complications with not being able to treat the rotations independently? Or is it better to take Δ large and to continue to work in the textbook regime?

The resolution to this question is provided by [15], where it is shown that not only is splitting the rotation still beneficial in the finite setting, and in addition that is beneficial to split the rotation *as much as possible*. Even though one enters the "counter-intuitive regime" where the different rotations interact with each other, the computation still proceeds most efficiently with maximal splitting.

2.3.5 Rotation-counter rotation test to measure computational power

We now consider the "simplest test" where one could showcase the computational power of finite MBQC resources. Namely, we perform the following protocol:

1. Prepare a ground state $|\phi(\alpha)\rangle$ of the interpolation Hamiltonian $H(\alpha)$ as in Eq. (2.5).
2. Prepare the one-qubit (logical) input state of $|+\rangle$.
3. Implement what on the cluster state would be the composition of cancelling z-rotations, separated by an even distance Δ. In other words, implement $R_z(\beta)R_z(-\beta) = I$ by measurement in the eigenbasis of $O(\pm\beta)$ on qubits with even separation Δ.
4. Measure the expectation value $\langle X\rangle$ of the logical output qubit (denoted as $\langle\overline{X}\rangle$).

For the 4-ring this protocol is illustrated graphically in Fig. 2.11.

The idea is that at the cluster point of $\alpha = 0$ we expect $\langle\overline{X}\rangle = 1$ as the output state is just $|+\rangle$ as the result of the cancelling z-rotations. As we go away from the cluster state with $\alpha \neq 0$, we expect a drop in $\langle\overline{X}\rangle$ from effects of the aforementioned logical decoherence from the symmetry-breaking measurements of $O(\pm\beta)$. From here onward, we take $\beta = \pi/2$ as this yields the measurement furthest away from the symmetry respecting choice (note that $\beta = 0 \mod \pi$ would lead to $R_z(\beta) = I$ which would in fact respect the $\mathbb{Z}_2 \otimes \mathbb{Z}_2$ symmetry). The intuition is that the

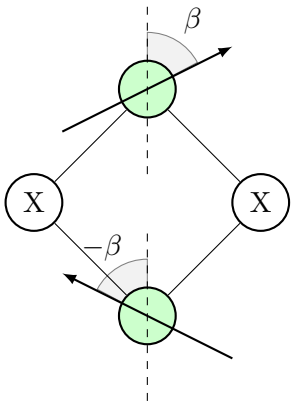

Figure 2.11: Visualization of the rotation-counter rotation MBQC protocol. A ring is prepared in the state $|\phi(\alpha)\rangle$. We input a $|+\rangle$ state, then perform measurements $O(\pm\beta)$ on qubits 1/3 (with rotations separated by distance $\Delta = 2$) and wire basis measurements on qubits 2/4 before measuring the expectation value $\langle X\rangle$ of the resulting logical qubit state.

experiment is measuring the ability for states $|\phi(\alpha)\rangle$ to carry out rotations without decoherence; therefore the measurement of $\langle \overline{X} \rangle$ is intuitively a measure of the computational power of the state.

Using iTensor [23], A. Adhikary gives theoretical predictions for these expectation values as a function of the interpolation parameter α, the ring size N, and the rotation separation Δ. These predictions are provided in Figs. 2.12 and 2.13.

We note that in systems approaching the thermodynamic limit (e.g. for large system size $N = 400$, as seen in Fig. 2.12) that the curves reproduce the SPT-phase result; we see a clear separation of states that are computationally useful ($\alpha < \frac{\pi}{4}$) and states that are computationally useless ($\alpha > \frac{\pi}{4}$) with a phase transition at $\alpha = \frac{\pi}{4}$. In the small-system regime, the drop in computational power is not as steep as in the thermodynamic limit, but the curves of computational power follow a similar characteristic shape that tends to the thermodynamic limit result as N is taken to be large.

Also, we note the choice of boundary conditions for the above experiment, which has so far been an unexplained switch from the familiar formalism of MBQC on chains. The ultimate reason is that while the boundary effects are insignificant in the thermodynamic limit, for small system sizes the effects can be quite severe. One can point to the fact that a finite cluster chain has incomplete stabilizers of X_1Z_2 and $Z_{n-1}X_n$ at the chain boundaries. To avoid this effect, one can consider closing the chain into a ring by enforcing the stabilizers $Z_nX_1Z_2$ and $Z_{n-1}X_nZ_1$ (or operationally,

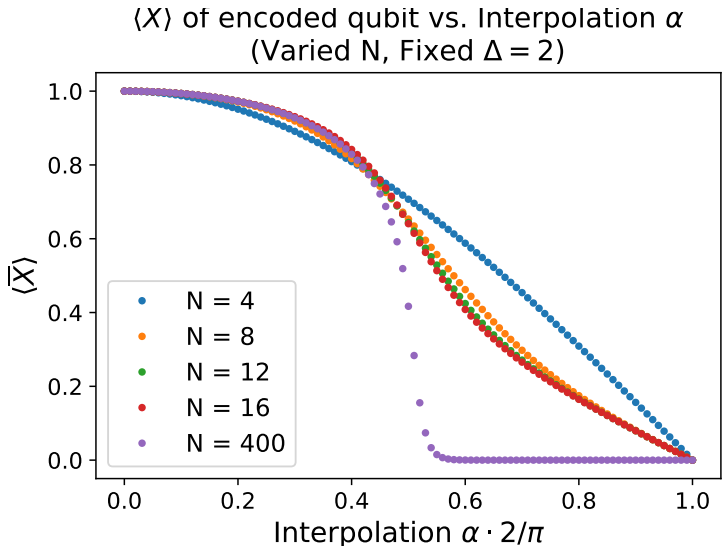

Figure 2.12: Theory plots of $\langle \overline{X} \rangle$ versus the interpolation parameter α for the rotation-counter rotation protocol. The plots were obtained using iTensor, for rings of size $N = 4, 8, 12, 16, 400$, rotation angle $\beta = \frac{\pi}{2}$ and rotation separation $\Delta = 2$. The calculations and plots are credited to A. Adhikary.

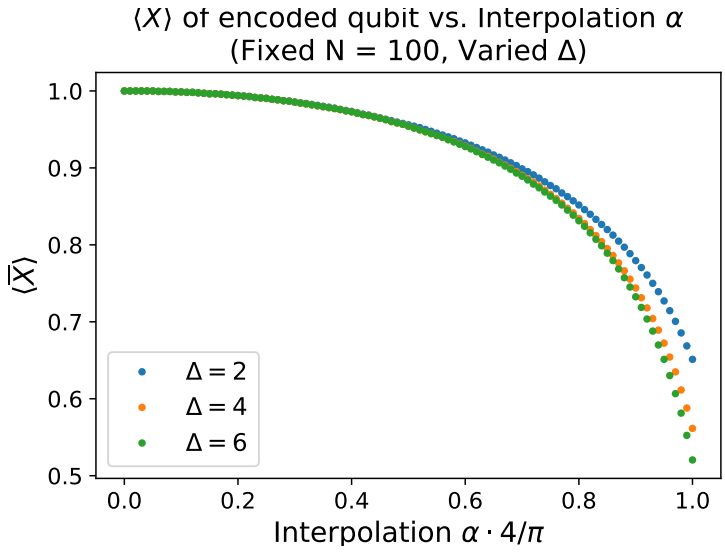

Figure 2.13: Theory plots of $\langle \overline{X} \rangle$ versus the interpolation parameter α for the rotation-counter rotation protocol. The plots were obtained using iTensor, for a ring of size $N = 100$, rotation angle $\beta = \frac{\pi}{2}$ and rotation separations $\Delta = 2, 4, 6$. The calculations and plots are credited to A. Adhikary.

by applying a entangling CZ gate between the two chain boundary qubits). We will return to this discussion when we discuss experimental implementations in the following chapter.

A theoretical calculation can be made in the limit that the separation distance is much larger than the correlation length, i.e. $\Delta \gg \eta(\alpha)$. In this regime, with rotation angle $\beta = \pi/2$ we have:

$$\left\langle \overline{X} \right\rangle = (2\nu_{01})^2 \tag{2.7}$$

where ν_{01} is the computational order parameter as introduced in Eq. (2.6). Note that the correlation length $\eta(\alpha)$ diverges at $\alpha = \frac{\pi}{4}$ (where the phase transition from the cluster phase to product phase would occur in the thermodynamic limit) and the numerics in Fig. 2.13 indeed demonstrate a deviation from this simple relation of $\left\langle \overline{X} \right\rangle$ and ν_{01}. There we see that as α approaches $\frac{\pi}{4}$ the curves differ depending on Δ, while in Eq. (2.7) the expectation value is Δ-independent.

There are two takeaways here that will motivate the remainder of the thesis. The first is the following: even in the finite regime, we observe the "robusteness" of quantum computational power. Though $\left\langle \overline{X} \right\rangle$ (which we take as a proxy for computational power in this experiment, with the direct relationship of Eq. (2.7) holding when $\Delta \gg \eta(\alpha)$) is maximized when $\alpha = 0$ (i.e. the cluster state), we still observe computationally useful states as we go away from the cluster state. The second is the following: we see a deviation from the simple theory prediction of (2.7) in the above numerical results due to the interplay of ν_{01} and correlation length $\eta(\alpha)$. This interplay is key to the "counter-intuitive regime" result of managing decoherence in MBQC in finite settings as previously discussed, and any experiment to demonstrate such decoherence management will need to be sensitive enough to be able to measure this interplay and hence deviation.

This gives us a concrete objective that we will pursue for the remainder of the thesis. Namely, can we reproduce the curves depicted in Fig. 2.12 on a physical quantum device? As per the first takeaway, this will allow us to experimentally demonstrate the robustness of computational power in MBQC resource states. Not only is this interesting from the theoretical perspective, but it also provides a new use case of NISQ devices to showcase interesting phenomenology concerning quantum computational power. As per the second takeaway, such a result would show that NISQ devices possess the fidelity to resolve small but intriguing theoretical effects. Hence, it would demonstrate that they are viable for future studies concerning not only the display of decoherence in MBQC, but optimal techniques for management of that decoherence (namely "divide-and-conquer" and "the counter-intuitive regime").

2.3.6 Creating resource states

One natural question that comes up in the discussion of the ground states $|\phi(\alpha)\rangle$ of the interpolation Hamiltonian in Eq. (2.5) is how does one go about generating these states on a quantum computer. Of course we know how to create the cluster state $|C\rangle$ and the product state $|+\rangle^{\otimes n}$ with relative ease, but generating the interpolated ground states appears to be a nontrivial problem.

Here we take our first steps to resolve this problem. First, we recognize that we can always find a unitary $U(\alpha)$ that connects two states in the same Hilbert space. So, let us connect $|\phi(\alpha)\rangle$ and the cluster state $|C\rangle$ as $|\phi(\alpha)\rangle = U(\alpha)|C\rangle$. Further, we can take $U(\alpha)$ to respect the $\mathbb{Z}_2 \otimes \mathbb{Z}_2$ symmetry of $H(\alpha)$. Now, we claim that we can find a simple representation of $U(\alpha)$; one that only consists of Pauli-X and Identity operators. The argument will rely on the fact that $U(\alpha)$ respects the above symmetry, and the fact that we can pull out cluster state stabilizers $Z_{i-1}X_iZ_{i+1}$ from $|C\rangle$.

Proof. It suffices to prove the claim for a Pauli operator P that satisfies $[P, IXIXIX\ldots] = [P, XIXIXI\ldots] = 0$ as $U(\alpha)$ can then be written as the weighted sum of such Pauli operators. If P consists solely of X and I operators already, then we are done. Suppose then that P does not consist of solely X and Is; then, P contains Zs or Ys (or both). However, since P commutes with the symmetries, the following conditions must hold:

1. There are in total an even number of Zs/Ys on odd sites.

2. There are in total an even number of Zs/Ys on even sites.

This is because since $XZ = -ZX$ and $XY = -YX$, there must be an even number of anti-commutations for the negatives to cancel and for P to commute with the symmetries.

To this end, let us pair up Z/Ys on odd sites (pairing up those that are the closest to each other) and let us pair up Z/Ys on even sites (again pairing up those that are the closest to each other). We now introduce an algorithm to deal with each pair and get rid of the Z/Ys.

For each pair on odd sites (one of $Z_{2n+1}Z_{2n+1+2k}, Y_{2n+1}Z_{2n+1+2k}, Z_{2n+1}Y_{2n+1+2k}, Y_{2n+1}Y_{2n+1+2k}$) we multiply P by the stabilizers $Z_{2n+1}X_{2n+2}Z_{2n+3}, Z_{2n+3}X_{2n+4}Z_{2n+5}, \cdots Z_{2n-1+2k}X_{2n+2k}Z_{2n+1+2k}$. In other words, multiply P by all the cluster stabilizers centered on even sites that fall in between the two offending Z or Y operators. This has the net effect of multiplying P by:

$$Z_{2n+1}X_{2n+2}I_{2n+3}X_{2n+4}\ldots I_{2n+2k-1}X_{2n+2k}Z_{2n+2k+1}.$$

This has the effect of removing the offending Z/Y terms at the $2n+1$ and $2n+2k+1$ sites. In

addition, it introduces no new Z/Y operators in between. Repeating this process for every pair of odd sites with offending Z/Y operators, we remove all Zs/Ys on odd sites.

Similarly, for each pair on even sites (one of $Z_{2n}Z_{2n+2k}, Y_{2n}Z_{2n+2k}, Z_{2n}Y_{2n+2k}, Y_{2n}Y_{2n+2k}$), we multiply P by the stabilizers $Z_{2n}X_{2n+1}Z_{2n+2}, Z_{2n+2}X_{2n+3}Z_{2n+4}, \cdots Z_{2n-2+2k}X_{2n-1+2k}Z_{2n+2k}$. In other words, multiply P be all the cluster stabilizers centered on odd sites that fall in between the two offending Z or Y operators. This has the net effect of multiplying P by:

$$Z_{2n}X_{2n+1}I_{2n+2}X_{2n+3}\ldots I_{2n+2k-2}X_{2n+2k-1}Z_{2n+2k}.$$

This has the effect of removing the offending Z/Y operators at the $2n$ and $2n+2k$ sites. In addition, it introduces no new Z/Y operators in between. Repeating this process for every pair of even sites with offending Z/Y operators, we remove all Zs/Ys on even sites.

Hence, we have given an algorithm such that our Pauli operator P modulo the cluster state stabilizers can be represented by purely X and I operators (as we have removed all the Z and Ys by the above algorithm). This concludes the proof.

So, we have shown that there exists a representation $T(\alpha)$ of $U(\alpha)$ that solely consists of Pauli X and I operators. Note that in the above construction that different Pauli parts in the weighted sum can be multiplied by different stabilizer operators; as such. the unitary of $U(\alpha)$ can be lost in this process. We will return to this consequence in a later portion of the thesis. We can make a further simplification; to first-order in perturbation theory, $T(\alpha)$ is local. Further, on a ring $T(\alpha)$ will be translation invariant, so its action will the same on each site. We can therefore write:

$$T(\alpha) = \bigotimes_{i=1}^{n} \left(a(\alpha)I_i + b(\alpha)X_i\right).$$

Given this simple form of $T(\alpha)$, classical variational algorithms can be used to solve for the coefficients $a(\alpha)$ and $b(\alpha)$. From previous work by D. Bondarenko, it has been shown that for small ring-sizes (up to $n = 6$), the $T(\alpha)|C\rangle$ found by classical optimization with the locality assumption is found to well approximate the exact ground state $|\phi(\alpha)\rangle$. However, we may desire more generalizable method for finding these coefficients, as for larger systems the calculation of $T(\alpha)$ becomes inaccurate under the locality assumption and intractable. To this end, we introduce a method to search for $T(\alpha)$ using a quantum device through the method of VQE.

2.4 Variational quantum eigensolvers

In this section, we introduce the theory of Variational Quantum Eigensolvers, or VQEs. VQEs are a a class of hybrid quantum-classical algorithms which have seen use in fields such as quantum chemistry [24]. The goal is to search for the unknown ground state $|\psi_0\rangle$ of some Hamiltonian H. To this end, these algorithm make use of variational principle, which states that for a Hamiltonian H with ground state energy E_0, any quantum state $|\psi\rangle$ satisfies:

$$\langle\psi|H|\psi\rangle \geq E_0.$$

Given this principle, we can consider some variational ansatz $|\psi(\vec{\theta})\rangle$ which depends on parameters $\vec{\theta}$. We can adjust these parameters to try to minimize $\langle\psi(\vec{\theta})|H|\psi(\vec{\theta})\rangle$, leading to an approximation of the ground state $|\psi_0\rangle$. This motivates the VQE algorithm as given in Table 2.1. We will discuss a specific variation on this general algorithm in the proceeding sections, which we can use to search for the $T(\alpha)$ operator experimentally.

VQE algorithm.

For a given Hamiltonian H for which we wish to approximate the ground state $|\psi_0\rangle$, execute the following steps.

1. Devise a variational anstatz $|\psi(\vec{\theta})\rangle$ for the ground state.
2. Create $|\psi(\vec{\theta})\rangle$ on a quantum device, with the preparation gates parameterized by $\vec{\theta}$.
3. Measure the energy $E = \langle\psi(\vec{\theta})|H|\psi(\vec{\theta})\rangle$ of the state.
4. Feed in the results into a classical computer to optimize the parameters $\vec{\theta}$.
5. Repeat steps 2-4 until E is minimized. The resulting $|\psi(\vec{\theta})\rangle$ yields an approximation to the ground state.

Table 2.1: VQE algorithm.

Chapter 3

Methods

In the previous section, we discussed the theory that forms the groundwork of the thesis. We also introduced in subsection 1.3.5 a test of computational power one could conduct. In this section, we flesh out the methods necessary to conduct this test experimentally, in the simplest setting of the 4-qubit ring.

3.1 Simulating MBQC on IBM devices

In this work, we have chosen to use the quantum devices provided by IBM as a) They have a widely used open-source SDK Qiskit for creating, simulating, and running quantum circuits and b) They offer free usage of small-scale quantum devices. IBM's quantum devices use superconducting qubits that execute quantum computation using the circuit model [25]. Therein enters the second layer of "simulation" in the title of this thesis; while MBQC simulates of the circuit model via adaptive measurements, we now wish to simulate a MBQC measurement protocol in the circuit model. The ideal simulation of the protocol in Section 1.3.5. would proceed as in Table 3.1.

However, there are logistical problems with all but the last step of this procedure at the outset:

(A) (Step 1) The IBM machines do not have universal connectivity of qubits; that is, it is not possible to apply entangling CZ gates between arbitrary pairs of qubits.

(B) (Step 2) The $T(\alpha)$ representation we have is a non-unitary operator; it therefore cannot in general be implemented efficiently via unitary quantum gates.

(C) (Step 3) The IBM machines operate in the circuit model, and therefore do not support measurement in arbitrary measurement bases; only the computational basis.

Protocol for measurement of $\langle \overline{X} \rangle_{\phi(\alpha)}$ on IBMQ device (ver 1).

1. Create a cluster state by applying $H^{\otimes 4}$ to the initial register of qubits $|0\rangle^{\otimes 4}$, and then applying CZ gates between qubits pairs 1-2, 2-3, 3-4, 1-4 to form the cluster ring $|C_{\text{ring}}\rangle$
2. Apply the $T(\alpha) = \bigotimes_{i=1}^{n} (a(\alpha) I_i + b(\alpha) X_i)$ transformation operator to each qubit as discussed in Section 1.3.6 to $|C_{\text{ring}}\rangle$ to obtain the ground state of interest $|\phi(\alpha)\rangle$.
3. Measure the first qubit in $O(\beta = \pi/2)$, the second qubit in X, the third qubit adaptively in $O((-1)^{s_2}(-\beta))$ where s_2 is the measurement outcome of the second qubit, and the fourth qubit in X.
4. Obtain the measurement outcome for X on the encoded qubit by interpreting the measurement outcomes from Step 3.
5. Repeat many times and average outcomes to obtain the expectation value $\langle X \rangle$ of the encoded qubit.

Table 3.1: Procedure (version 1) for measurement of $\langle \overline{X} \rangle$ for (4-qubit) ground state $|\phi(\alpha)\rangle$ of $H(\alpha)$ on an IBM circuit-model quantum computer.

(D) (Step 3) The IBM machines do not support adaptive measurements; hence we cannot adaptively change the measurement basis on the third qubit based on the outcome of the second qubit. For completeness, we note that while the devices do allow for intermediate measurements, conditional operations based on the outcomes of such intermediate measurements are not supported at this time. So effectively, we only have access to an all-at-once measurement at the end of the computation.

(E) (Step 4) We do not know how to interpret the measurement outcomes to extract the value of the logical X-measurement.

We address problems D/C/E here and address A/B in the proceeding sections.

Solution to problem D. Since we cannot adaptively measure, we post-select on measurement outcomes; we measure in $O(\beta)$ on the first qubit, X on the second qubit, $O(-\beta)$ on the third qubit,

and X on the fourth qubit, and if we find that $s_2 = 1$ (i.e. the "wrong" measurement outcome that would flip the third measurement) we discard that run of the experiment.

Solution to problem C. We recall the projector-unitary identity as in Eq. (2.4), which tells us that for a measurement observable O (with eigenvalues ± 1) and unitary U:

$$\Pi_O U = \Pi_{U^\dagger O U}.$$

Previously, we used this relation to show that applying a unitary and then measuring could be equivalently attained with one measurement. We now use the reverse; that one measurement can be equivalent to applying a unitary (which we now have access to as we work with a circuit-model quantum computer) and then measuring in Z. Therein, suppose O' is the observable whose eigenbasis we wish to measure in, but we only have access to measuring in the computational (Z) basis. We set $O = Z$, $U^\dagger O U = O'$ and then solve for what U should be. If $|v_+\rangle, |v_-\rangle$ are the ± 1 eigenstates of O', then we find from $O' = U^\dagger Z U$ that

$$U = |0\rangle\langle v_+| + |1\rangle\langle v_-| \tag{3.1}$$

Note that for the measurement bases of interest of X and $O(\pm\beta)$, this amounts to $\Pi_X = \Pi_Z H$ and $\Pi_{O(\pm\beta)} = \Pi_X R_z(\pm\beta) = \Pi_Z H R_z(\pm\beta)$.

Solution to problem E. We can carry out an explicit calculation of the MBQC protocol on a 4-qubit cluster ring to determine what $\langle X \rangle$ should be for the encoded state. Given an input state of $|\psi_{\text{in}}\rangle = |+\rangle_1$, the circuit to be executed is provided by Fig. 3.1(a). This circuit can then be simplified via the half-teleportation and z-rotation identities to yield the circuit in Fig. 3.1(b).

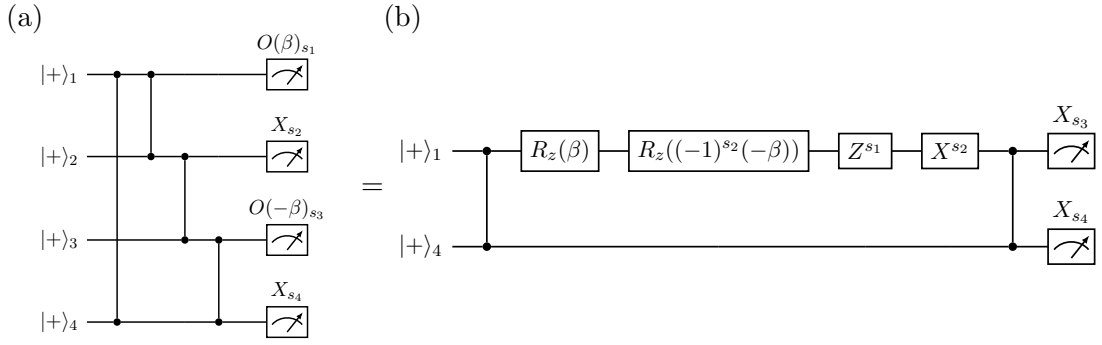

Figure 3.1: Circuit for rotation-counter rotation protocol on 4-qubit cluster ring (a) and subsequent simplification using half-teleportations (b).

We then use the identity that the two qubit cluster state is a locally Hadamard rotated bell pair, where:

$$|C_2\rangle = CZ_{1,2}|{+}{+}\rangle = (I_1 \otimes H_2)|B_{00}\rangle.$$

Combining these with the projector identity of $\Pi_X = \Pi_Z H$ and the conjugation identity of $HZH = X$, we obtain the circuit in Fig. 3.2.

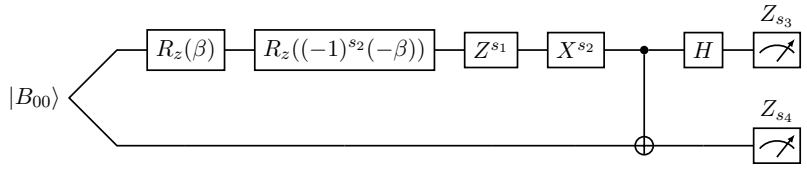

Figure 3.2: Simplified version of circuit in Fig. 3.1 for the rotation counter-rotation protocol on the 4-qubit cluster ring. The input is written as a Bell state, and the combination of the CX and Hadamard gate with the computational basis measurements realizes a Bell measurement.

The circuit above provides us with a physical interpretation of MBQC on a ring. In this setting, the input is realized as the Bell state $|B_{00}\rangle$. Then, the first qubit of the Bell pair is selectively evolved through the sequence of measurements (with byproduct operators), as would occur in the standard mechanism of MBQC on a chain. Finally, the pair of qubits is measured in the Bell basis.

For our experimental realization of the protocol, we post select on $s_2 = 0$. The measurement outcome of our interest, which is the outcome on the first qubit of the Bell pair (the qubit that undergoes evolution) is then determined by $s_1 + s_3$, which can seen by propogating the Z^{s_1} byproduct to the final measurement. Explicitly, an outcome of $s_1 + s_3 = 0$ corresponds to a logical X outcome of 1, and the outcome of $s_1 + s_3 = 1$ corresponds to a logical X outcome of -1. It then follows that $\langle \overline{X} \rangle = \langle (-1)^{s_1+s_3} \rangle$. The fully simplified circuit is shown in Fig. 3.3 below.

It is evident from the fully simplified circuit that $s_1 + s_3 = 0$ always for the cluster state as $R_z(\beta)$ and $R_z(-\beta)$ perfectly cancel and the subsequent Bell measurement on $|B_{00}\rangle$ returns the outcome 00. Hence, we find that $\langle \overline{X} \rangle = \langle (-1)^{s_1+s_3} \rangle = 1$ as we expect. For MBQC on states away from the cluster state (i.e. $|\phi(\alpha)\rangle$ for $\alpha > 0$), we find that the rotations $R_z(\pm\beta)$ are no longer implemented without logical decoherence, and hence do not cancel to the identity as in the cluster case. However, the final measurement outcome of interest is still determined in the same way as the cluster case to be $s_1 + s_3$. Hence, the expectation value of X for the logical qubit in the rotation-counter rotation

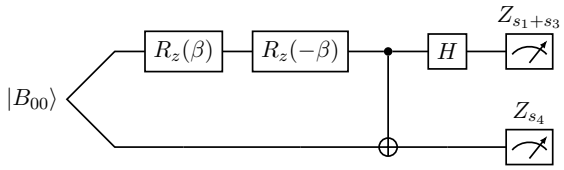

Figure 3.3: Fully simplified circuit for the rotation-counter rotation protocol on 4-qubit cluster ring, using post-selection condition of $s_2 = 0$ and propagating the Z^{s_2} gate past the Hadamard and into the measurement.

protocol is concluded to be given by:

$$\left\langle \overline{X} \right\rangle = \left\langle (-1)^{s_1+s_3} \right\rangle . \tag{3.2}$$

3.2 Solution to problem A - Local complementation

As was noted in the previous section, the available IBM devices do not have universal connectivity; entangling gates cannot be applied to arbitrary pairs of qubits. In particular, the smallest-qubit architectures of our interest have linear rather than periodic connectivity, as shown in Fig. 3.4 below.

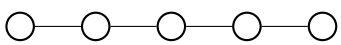

Figure 3.4: Visualization of linear architecture of the 5-qubit quantum computers *ibmq_bogota*, *ibmq_santiago*, and *ibmq_manila*. Circles represent qubits and lines represent pairs for which two-qubit gates (i.e. CX gates) may be applied.

We wish to prepare the 4-qubit cluster ring, so this architecture is less than optimal. In principle, we could prepare the 4-qubit cluster chain, swap the states of the first and third qubits through a series of SWAP gates, apply an entangling gate to close the ring, and then SWAP back. However, two qubit gates have higher error-rates than single-qubit operations; we therefore want to minimize the number of two qubit gates we apply. Given that a SWAP gate is equivalent to $CZ_{1,2}CZ_{2,1}CZ_{1,2}$ the closing of the ring at first seems to incur a cost of 12 additional 2-qubit gates, which is not optimal.

Fortunately, there exists a way to interchange between graph state architectures of certain types through use of local gates only, in a method known as local complementation [26]. In [26] it is

shown that through a sequential application of the (local) operator:

$$U_a(G) = \sqrt{-iX_a} \prod_{b \in N_a} \sqrt{iZ_b} \tag{3.3}$$

that it is possible to convert between the cluster chain and cluster ring. Note that N_a here represents the neighbours of the qubit a in the graph state. This sequence is outlined in Fig. 3.5 below.

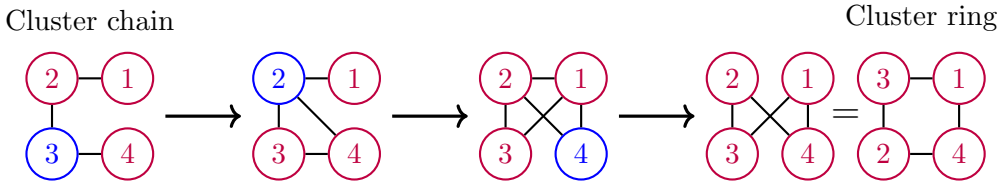

Figure 3.5: Visualization of local complementation sequence to convert from the 4-qubit cluster chain to ring. At each step, the operator in Eq. 3.3 is applied, with a taken to be the vertex in blue.

We therefore in our experiments can generate a 4-qubit cluster chain and then apply a sequence of inexpensive/less error-prone local unitary gates to transform this into a ring. We also note the small detail of qubits 2/3 switching their positions through the complementation. We do not need to apply a SWAP gate to account for this, but rather can keep track of the relabelling in the circuit and in post-processing the outcomes thereafter.

Before we move onto addressing the final (and most subtle) problem, the protocol in its current state is given in Table. 3.2, with graphical representation given in Fig. 3.6. Of course, this circuit is still not the one we can actually run due to the sticking issue of the non-unitarity of $T(\alpha)$, which we now address.

3.3 Solution to problem B - Pushing $T(\alpha)$ to the measurement

3.3.1 Associativity trick

Finally, we will now resolve the issue of the inefficiency of implementing $T(\alpha)$ arising from its non-unitarity. First, we note that as per the realization that $\langle \overline{X} \rangle = \langle (-1)^{s_1+s_3} \rangle$ and $s_2 = s_4 = 0$, we really are just measuring the four probabilities $p(s_1 = 0, s_3 = 0), p(s_1 = 0, s_3 = 1), p(s_1 = 1, s_3 = 0)$, and $p(s_1 = 1, s_3 = 1)$. Denote by $|O(\pm\beta)_\pm\rangle$ the positive/negative eigenstates of $O(\pm\beta)$. Then the

Protocol for measurement of $\langle \overline{X} \rangle_{\phi(\alpha)}$ on IBMQ device (ver 2).

1. Prepare the cluster chain on $|0\rangle^{\otimes 4}$ by applying $H^{\otimes 4}$ and applying CZ gates on pairs 1-2, 2-3, 3-4 as allowed by the architecture.
2. Apply the local complementation procedure as dictated by Eq. (3.3) and Fig. 3.5 to convert from a cluster chain to a ring.
3. Apply the $T(\alpha) = \bigotimes_{i=1}^{n} (a(\alpha) I_i + b(\alpha) X_i)$ transformation operator to each qubit as discussed in Section 1.3.6 to $|C_{\text{ring}}\rangle$ to obtain the ground state of interest $|\phi(\alpha)\rangle$.
4. Apply H to qubits 2/4, $R_z(\beta)H$ to qubit 1, and $R_z(-\beta)H$ to set up measurements in the desired bases.
5. Physically measure all 4-qubits in the computational basis.
6. If $s_2 = 1$, then throw away that run of the experiment. Otherwise, keep the measured outcome, and calculate the logical expectation value as $\langle \overline{X} \rangle = \langle (-1)^{s_1 + s_3} \rangle$.

Table 3.2: Procedure (version 2) for measurement of $\langle \overline{X} \rangle$ for (4-qubit) ground state $|\phi(\alpha)\rangle$ of $H(\alpha)$ on an IBM circuit-model quantum computer.

post-measurement states $|v_{\pm,\pm}\rangle$ are given by:

$$|v_{\pm,\pm}\rangle = |O(\beta)_{\pm}\rangle_1 |+\rangle_2 |O(-\beta)_{\pm}\rangle_3 |+\rangle_4 \tag{3.4}$$

and therefore the probabilities of obtaining this post measurement state is given simply by the Born rule to be:

$$p(s_1 = 0/1, s_3 = 0/1) = |\langle v_{\pm,\pm} | \phi(\alpha) \rangle|^2$$

We now observe, using that $|\phi(\alpha)\rangle = T(\alpha)|C\rangle$ and associativity that:

$$p(s_1 = 0/1, s_3 = 0/1) = |\langle v_{\pm,\pm} | (T(\alpha)|C\rangle)|^2 = |(\langle v_{\pm,\pm}| T(\alpha))|C\rangle|^2 = |\Big\langle T^{\dagger}(\alpha) v_{\pm,\pm} \Big| C \Big\rangle|^2$$

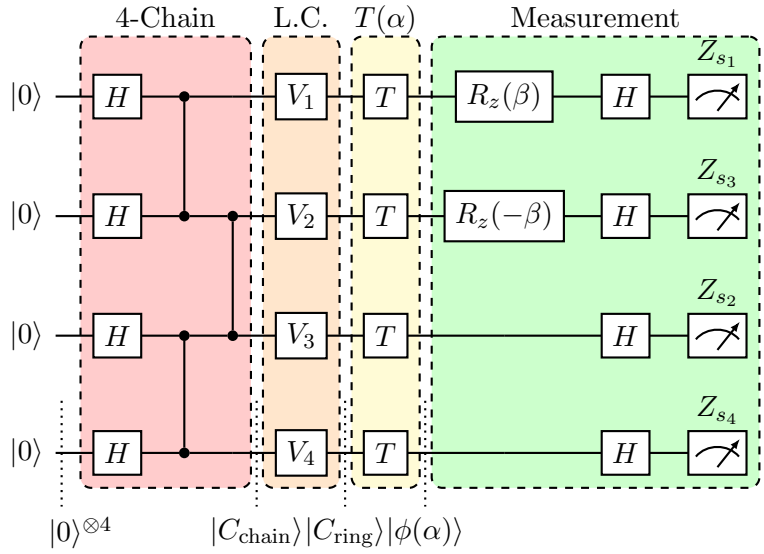

Figure 3.6: Circuit realization of the rotation-counter rotation protocol as described in Section 2.3.5.. We first prepare the 4-qubit cluster chain (red), then form the 4-qubit cluster ring (orange) via local complementation (noting the relabelling of qubits 2/3). We then apply the $T(\alpha)$ operator to obtain the ground state of interest $|\phi(\alpha)\rangle$ (yellow). We then apply $R_z(\pm\beta)$ to qubits 1/3 to produce a rotation aand counter rotation, and apply Hadamards to qubits 2/4 to produce quantum wire 2/4 (green). The value of $\langle\overline{X}\rangle$ is obtained by taking $\langle(-1)^{s_1+s_3}\rangle$.

so we conclude:

$$p(s_1 = 0/1, s_3 = 0/1) = |\langle v_{\pm,\pm}|\phi(\alpha)\rangle|^2 = |\Big\langle T^\dagger(\alpha)v_{\pm,\pm}\Big|C\Big\rangle|^2. \tag{3.5}$$

the above derivation is mathematically trivial, but is profound. Namely, it tells us that the probability of obtaining post measurement state $|v_{\pm,\pm}\rangle$ with pre-measurement state $|\phi(\alpha)\rangle$ is equivalent to obtaining post measurement state $|T^\dagger(\alpha)v_{\pm,\pm}\rangle$ with pre-measurement state $|C\rangle$ (the cluster state). In other words, our problem decomposes; instead of having to worry about preparing $|\phi(\alpha)\rangle = T(\alpha)|C\rangle$ on the quantum device (which could be inefficient), we can (easily) prepare the cluster state and just change our measurement basis instead, obtaining the same results for the probabilities and hence for $\langle\overline{X}\rangle$.

3.3.2 Non-orthogonal measurements

The above trick does not quite solve all of our problems, for the following reason: non-unitary operators do not in general preserve angles. We here will discuss a simpler example to show why this could be problematic. Suppose we have an orthonormal basis $\mathcal{B}_0 = \{|k_+\rangle, |k_-\rangle\}$. We then consider applying some non-unitary $T^\dagger$ to both of these states, giving us $T^\dagger|k_+\rangle, T^\dagger|k_-\rangle$, which we want to find the probabilities of obtaining as post-measurement states. $T^\dagger$ is not in general norm preserving, so we first normalize; we define $|n_\pm\rangle = \frac{T^\dagger|k_\pm\rangle}{\langle k_\pm|TT^\dagger|k_\pm\rangle}$ which are indeed normalized. However, $|n_+\rangle, |n_-\rangle$ are not in general orthogonal, as $TT^\dagger \neq I$ and so generally:

$$\langle n_+|n_-\rangle = \frac{\langle k_\pm|TT^\dagger|k_\pm\rangle}{\langle k_+|TT^\dagger|k_+\rangle\langle k_-|TT^\dagger|k_-\rangle} \neq \frac{\langle k_+|k_-\rangle}{\langle k_+|TT^\dagger|k_+\rangle\langle k_-|TT^\dagger|k_-\rangle} = 0$$

Therefore $\{|n_+\rangle, |n_-\rangle\}$ does not in general form an orthonormal basis. However, we require an orthonormal basis to carry out quantum measurements!

We rectify this situation as follows: We consider the two orthonormal bases given by $\mathcal{B}_1 = \{|n_+\rangle, |n_+\rangle^\perp\}$, $\mathcal{B}_2 = \{|n_-\rangle, |n_-\rangle^\perp\}$ where $|\psi\rangle^\perp$ is a normalized ket orthogonal to $|\psi\rangle$. For $|\psi\rangle = a|0\rangle + b|1\rangle$, $|\psi\rangle^\perp = b^*|0\rangle - a^*|1\rangle$.

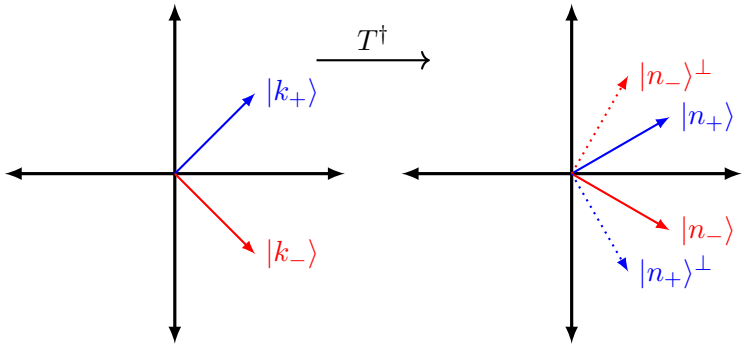

Figure 3.7: Visualization of application of a non-unitary $T^\dagger$ to an orthonormal basis $\{|k_+\rangle, |k_-\rangle\}$. Since non-unitary operators do not preserve inner products, the resulting states $T^\dagger|k_\pm\rangle$ are not generally normalized nor orthogonal. However, we can normalize to form $|n_\pm\rangle$, and then define orthogonal vectors to these transformed states to form two separate bases.

We can then do two experiments; one measuring in the $\mathcal{B}_1$ basis and one measuring in the $\mathcal{B}_2$ basis. Then, denote by p_+ the probability of measuring $|n_+\rangle$ in the first experiment and by p_- the

probability of measuring $|n_-\rangle$ in the second experiment. We can then calculate:

$$p'_+ = \frac{p_+}{p_+ + p_-}, \quad p'_- = \frac{p_-}{p_+ + p_-}$$

and these probabilities p'_+, p'_- are precisely what the probabilities of measuring $|n_+\rangle \sim T^\dagger|k_+\rangle$ and $|n_-\rangle \sim T^\dagger|k_-\rangle$ would be if we were able to perform a single experiment measuring in $\{|n_+\rangle, |n_-\rangle\}$.

Let us return back from this illustrative example and consider the states at hand. We want to measure in the basis $\{T^\dagger(\alpha)|v_{\pm,\pm}\rangle\}$ where $|v_{\pm,\pm}\rangle = |O(\beta)_\pm\rangle_1|+\rangle_2|O(-\beta)_\pm\rangle_3|+\rangle_4$ as before. Note that since the coefficients $a(\alpha), b(\alpha)$ in $T(\alpha) = \bigotimes_{i=1}^n (a(\alpha)I_i + b(\alpha)X_i)$ are real, we have that $T^\dagger(\alpha) = T(\alpha)$. Looking at the action of $T_i(\alpha) = a(\alpha)I_i + b(\alpha)X_i$ on $|+\rangle$, we have:

$$T_i(\alpha)|+\rangle = (a(\alpha)I + b(\alpha)X)|+\rangle = (a(\alpha) + b(\alpha))|+\rangle$$

so other than a renormalization of the state by $\frac{1}{a(\alpha)+b(\alpha)}$, qubits 2/4 are unchanged by T (and are still orthogonal to $|-\rangle$); hence for these qubits the above construction of forming a new ONB need not be applied. For the action of $T_i(\alpha)$ on $|O(\beta)_\pm\rangle$, we are less fortunate:

$$\begin{aligned} T_i(\alpha)|O(\beta)_\pm\rangle &= (a(\alpha)I + b(\alpha)X)\left(\pm\frac{e^{i\beta}}{\sqrt{2}}|0\rangle + \frac{1}{\sqrt{2}}|1\rangle\right) \\ &= \frac{\pm a(\alpha)e^{i\beta} + b(\alpha)}{\sqrt{2}}|0\rangle + \frac{\pm b(\alpha)e^{i\beta} + a(\alpha)}{\sqrt{2}}|1\rangle \end{aligned}$$

we find that $T_i(\alpha)|O(\beta)_+\rangle$ and $T_i(\alpha)|O(\beta)_-\rangle$ are not orthogonal to each other. Therefore, for qubits 1 and 3 we define:

$$|n(\pm\beta)_\pm\rangle = \frac{T_i(\alpha)|O(\pm\beta)_\pm\rangle}{\langle O(\pm\beta)_\pm|T_i^2(\alpha)|O(\pm\beta)_\pm\rangle} \tag{3.6}$$

And construct orthogonal kets $|n(\pm\beta)_\pm\rangle^\perp$. Since we now have two non-orthogonal measurements, we require $2^2 = 4$ different experiments in different measurement bases. These four bases are (omitting the $|+\rangle$ qubits on 2 and 4 which are the same for each bases):

(a) $\{|n(\beta)_+\rangle_1|n(-\beta)_+\rangle_3, |n(\beta)_+\rangle_1^\perp|n(-\beta)_+\rangle_3, |n(\beta)_+\rangle_1|n(-\beta)_+\rangle_3^\perp, |n(\beta)_+\rangle_1^\perp|n(-\beta)_+\rangle_3^\perp\}$

(b) $\{|n(\beta)_+\rangle_1|n(-\beta)_-\rangle_3, |n(\beta)_+\rangle_1^\perp|n(-\beta)_-\rangle_3, |n(\beta)_+\rangle_1|n(-\beta)_-\rangle_3^\perp, |n(\beta)_+\rangle_1^\perp|n(-\beta)_-\rangle_3^\perp\}$

(c) $\{|n(\beta)_-\rangle_1|n(-\beta)_+\rangle_3, |n(\beta)_-\rangle_1^\perp|n(-\beta)_+\rangle_3, |n(\beta)_-\rangle_1|n(-\beta)_+\rangle_3^\perp, |n(\beta)_-\rangle_1^\perp|n(-\beta)_+\rangle_3^\perp\}$

(d) $\{|n(\beta)_-\rangle_1|n(-\beta)_-\rangle_3, |n(\beta)_-\rangle_1^\perp|n(-\beta)_-\rangle_3, |n(\beta)_-\rangle_1|n(-\beta)_-\rangle_3^\perp, |n(\beta)_-\rangle_1^\perp|n(-\beta)_-\rangle_3^\perp\}$

Denoting j_1, j_2, j_3, j_4 as the outcomes on the four qubits in the experiments above, we are interested in the probability $p(j_1 = j_3 = 0)$ of getting the first outcome in the basis (again post selecting on experiments where $j_2 = 0$). Each of these probabilities corresponds to a probability that we wanted to measure in the original experiment. Namely, $p(j_1 = j_3 = 0)$ in experiment (a) corresponds to the probability that $p(s_1 = s_3 = 0)$, and analogously experiment (b) gives the probablity that $p(s_1 = 0, s_3 = 1)$, experiment (c) gives the probability that $p(s_1 = 1, s_3 = 0)$ and experiment (d) gives the probability that $p(s_1 = s_3 = 1)$.

In accordance with applying a unitary to adjust the measurement bases, the corresponding unitaries for the above measurement bases as given by Eq. (3.1) are denoted:

$$N_\alpha(\beta, \pm) = |0\rangle\langle n(\beta)_\pm| + |1\rangle\langle n(\beta)_\pm|^\perp. \tag{3.7}$$

Chapter 4

Results - Algorithms

4.1 Circuits and post-processing algorithm rotation-counter rotation experiment

Having now resolved all of the problems with our initial formulation in Table 3.1, we give a complete and fully executable procedure for the measurement of the expectation value $\langle \overline{X} \rangle$ for the rotation-counter rotation protocol as carried out on the 4-qubit (ring) $|\phi(\alpha)\rangle$. This is provided in Table 4.1, with visualized circuits in Fig. 4.1.

Protocol for measurement of $\langle \overline{X} \rangle_{\phi(\alpha)}$ on IBMQ device (ver 3).

For a given value of the interpolation parameter α, and corresponding coefficents $a(\alpha), b(\alpha)$ of the transformation operator $T(\alpha)$, execute the following:

1. For many times, run the four circuits given in Fig. 4.1. In each, the following occurs:
   (a) The cluster chain is prepared $|0\rangle^{\otimes 4}$ by applying $H^{\otimes 4}$ and applying CZ gates on pairs 1-2, 2-3, 3-4 as allowed by the architecture.
   (b) The local complementation procedure as dictated by Eq. (3.3) and Fig. 3.5 is applied to convert from a cluster chain to a ring.
   (c) H is applied to qubits 2/4 to set up for a wire basis measurement. A combination of $N_\alpha(\beta = \pi/2, \pm)$ and $N_\alpha(-\beta = -\pi/2, \pm)$ (defined by Eq. 3.7) are applied to qubits 1/3 respectively to set up the non-orthogonal measurement protocol as described in Section 3.3.
   (d) The qubits are physically measured in the computational basis.
   (e) Any outcomes with $j_2 = 1$ are discarded due to post selection.
   (f) From the remaining outcomes, compute the probability $p(j_1 = j_3 = 0)$.
2. Denote by p_{++} the the probability of $p(j_1 = j_3 = 0)$ found in the first step for $N(\beta, +)$ on qubit 1 and $N(-\beta, +)$ on qubit 3, with analogous definitions of p_{+-}, p_{-+}, and p_{--}. Calculate $P = p_{++} + p_{+-} + p_{-+} + p_{--}$ as the normalization factor.
3. Define $p'_{++} = p_{++}/P$ and analogously for $p'_{+-}, p'_{-+}, p'_{--}$. Note the correspondence of $p(s_1 = s_3 = 0) = p'_{++}$, $p(s_1 = 0, s_3 = 1) = p'_{+-}$, $p(s_1 = 1, s_3 = 0) = p'_{-+}$, $p(s_1 = 1, s_3 = 1) = p'_{--}$.
4. Calculate $\langle \overline{X} \rangle$ as:

$$\langle \overline{X} \rangle = \langle (-1)^{s_1 + s_3} \rangle = p'_{++} + p'_{--} - p'_{+-} - p'_{-+}.$$

Table 4.1: Procedure (complete) for measurement of $\langle \overline{X} \rangle$ for (4-qubit) ground state $|\phi(\alpha)\rangle$ of $H(\alpha)$ on an IBM circuit-model quantum computer.

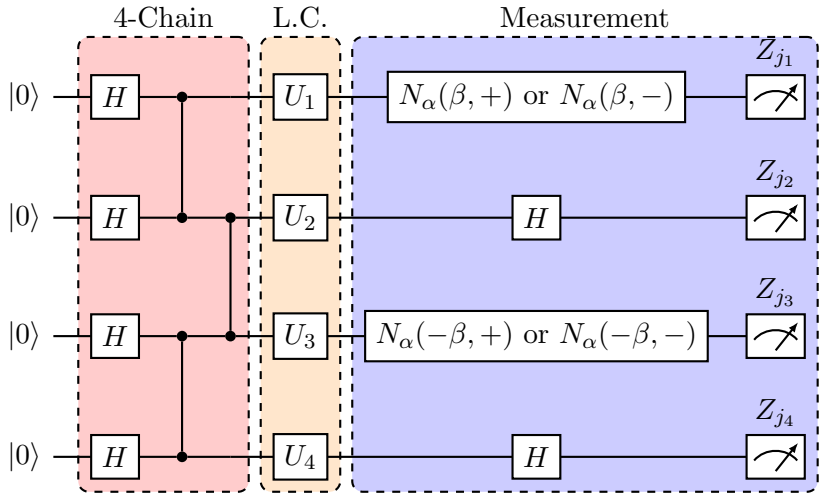

Figure 4.1: The 4 circuits used for measurement of the encoded $\langle \overline{X} \rangle$ on the 4-qubit ring $|\phi(\alpha)\rangle$. We prepare the 4-qubit cluster chain (red), then form the 4-qubit cluster ring (orange) via local complementation (noting the relabelling of qubits 2/3). We then have four sets of $N_\alpha(\beta, \pm)$ operators that we apply to conduct the non-orthogonal measurement.

4.2 VQE to find $T(\alpha)$/VQE algorithm for $\langle X_i \rangle_\theta$

Currently, our transformation operator $T(\alpha)$ is found via classical variational optimization. However, we have two reasons for wanting to find $T(\alpha)$ on a quantum computer. Firstly, the search for $T(\alpha)$ becomes classically intractable for large system sizes. Secondly, the project would be closer to true quantum mechanical demonstration by cutting out a currently classical component. Therein, we consider a variant of the VQE algorithm as described in Section 2.4 on the IBM devices. We therefore require a variational ansatz state $|\Psi(\theta)\rangle$ which approximates $|\Phi(\alpha)\rangle = T(\alpha)|C\rangle$ (where $|C\rangle$ is a cluster ring of even size). Therein, we select the ansatz:

$$|\Psi(\theta)\rangle = T'(\theta)|C\rangle = \left(\bigotimes_{i=1}^{n} \cos(\theta) I_i + \sin(\theta) X_i \right) |C\rangle = \bigotimes_i T'_i(\theta)|C\rangle. \tag{4.1}$$

This ansatz has many of the desired properties; namely that it shares the translation invariance and $\mathbb{Z}_2 \otimes \mathbb{Z}_2$ symmetry of $H(\alpha)$, it agrees with a perturbation theory theory to linear order, and it predicts the existence of a phase transition (much like we see with $|\phi(\alpha)\rangle$.

We have that $T'(\theta) = (\bigotimes_i \cos(\theta) I_i + \sin(\theta) X_i)$ approximates $T(\alpha)$ best when the energy is minimized. The per-site energies are given by:

$$E_i = -\cos(\alpha) \langle K_i \rangle_\theta - \sin(\alpha) \langle X_i \rangle_\theta \tag{4.2}$$

Where $K_i = Z_{i-1} X_i Z_{i+1}$ is the cluster state stabilizer at site i, and X_i is the magnetic field at site i. So for each α we find a θ for which E_i is minimized, allowing us to find θ as a function of α and therefore learn a form of $T(\alpha)$ using a quantum variational algorithm.

We therefore wish to construct circuits to conduct measurements of $\langle X_i \rangle_\theta$ and $\langle K_i \rangle_\theta$ for varying values of θ. Note that due to the translation invariance of $|\Psi(\theta)\rangle$, it suffices to consider measure and minimize for a single site i (as the result will be the same for every site). WLOG we can then consider measurements of $\langle X_1 \rangle_\theta$ and $\langle K_2 \rangle_\theta = \langle Z_1 X_2 Z_3 \rangle_\theta$. One roadblock that stands in our way follows from the previous discussion of non-unitarity; $T'(\theta)$ as given in (4.1) is non-unitary, so implementing and then measuring this state should be inefficient. However, there turns out to be a drastic simplification in the measurement of $\langle X_1 \rangle_\theta$. The algorithm for measuring it is given below in Table 4.2. The proceeding algorithm, its derivation, and its proof of correctness are attributed to R. Raussendorf.

Protocol for the measurement of the magnetic field.

1. For many times, run the simple one qubit circuit

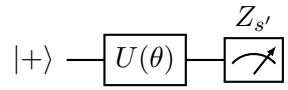

   where $U(\theta) \cong \begin{bmatrix} \cos\theta & \sin\theta \\ -\sin\theta & \cos\theta \end{bmatrix}$. Group the simulation outcomes s'_i into batches of size 2.

2. Pick a pair of batches (b, b'). If it holds that $\sum_{i\in b} s'_i \mod 2 = \sum_{j\in b'} s'_j \mod 2 = 0$, then keep both batches; otherwise discard them. Repeat until all batches have been checked.

3. From the remaining batches, approximate the magnetic field as $\langle X_i\rangle_\theta = \frac{1}{2N}\sum_b \sum_{i\in b} s'_i$, where N is the number of batches remaining after step 2.

Table 4.2: Procedure for obtaining the expectation value of the local magnetic field term for the ansatz state of Eq (4.1).

Proof of correctness

A straight quantum-mechanical calculation of the magnetic field yields:

$$\langle X_{\mathrm{i}}\rangle_\theta = \langle X_1\rangle_\theta = \langle\Psi(\theta)|X_1 I_2 I_3 I_4|\Psi(\theta)\rangle = \frac{2x}{1+x^2}. \tag{4.3}$$

Where $x = 2\sin\theta\cos\theta$. A derivation of this formula is found in the appendix. If the algorithm can reproduce this value, then it is correct. It does so as follows. The uncorrelated probabilities $p(0), p(1)$ of obtaining the positive/negative outcomes in step 1 of the algorithm can be calculated to be:

$$p(0) = \frac{(\cos\theta + \sin\theta)^2}{2} = \frac{1+x}{2}, \quad p(1) = 1 - p(0) = \frac{1-x}{2}$$

Therefore the probability that one batch passes the parity test in step 2 is calculated to be:

$$p_{+,1} = p(0)^2 + p(1)^2 = \frac{1+x^2}{2}$$

Therefore the probability p_+ that both batches pass the parity tests is:

$$p_+ = (p_{+,1})^2 = \left(\frac{1+x^2}{2}\right)^2$$

We now consider the probabilities p_{++} for passing both parity tests and having the spin being up (in the zero/positive state) and the probability p_{-+} for passing both parity tests having the spin being down (in the one/negative state). With the above, these probabilities are

$$p_{++} = p(0)^2 p_{+,1} = \left(\frac{1+x}{2}\right)^2 \frac{1+x^2}{2}, \quad p_{-+} = p(1)^2 p_{+,1} = \left(\frac{1-x}{2}\right)^2 \frac{1+x^2}{2}$$

The expectation value outputted by the procedure is thus

$$\langle X_i \rangle_\theta = \frac{p_{++} - p_{-+}}{p_+} = \frac{2x}{1+x^2}$$

This agrees with the quantum-mechanical value of Eq. (4.3).

Circuit derivation

The straightforward circuit for the measurement of the magnetic field is displayed in Fig. 4.2.

The circuit in Fig. 4.2 is made of two parts, namely the creation of the cluster states and the probabilistic implementations of the non-unitary transformation operator $T_i'(\theta) = \cos\theta I_i + \sin\theta X_i$. We note that the latter is what yields an unwieldy circuit of 8 qubits to measure something on a 1 qubit state, as the implementation of a non-unitary operation requires a measurement rather than an application of a unitary gate. This implementation is realized as the circuit in Fig. 4.3, which implements the operation:

$$\begin{aligned} T_i &= \cos\theta I_i + \sin\theta X_i \\ \bar{T}_i &= X_i(\cos\theta I_i - \sin\theta X_i) \end{aligned} \tag{4.4}$$

If $s_{z,i} = 1$ (i.e. the ancilla measurement gives the negative outcome) then the byproduct X_i is absorbed in the subsequent X-measurement, but the minus sign is a probabilistic effect that sticks.

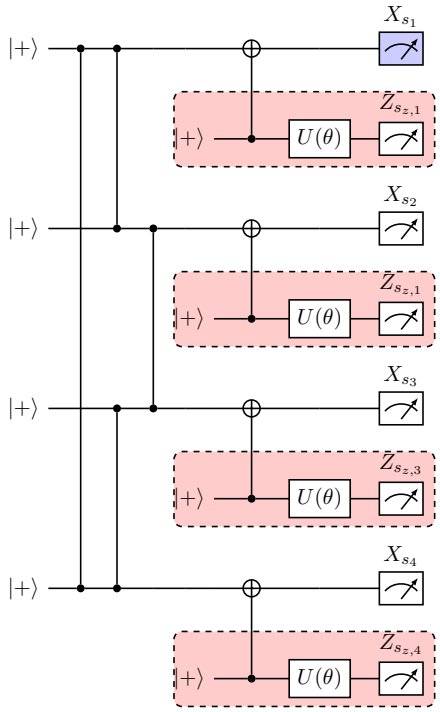

Figure 4.2: Unsimplified circuit for measurement of the expectation value $\langle X_i \rangle_\theta = \langle X_1 \rangle_\theta$ for the VQE algorithm. The ancilla measurements (red) correspond to the probabilistic application of $T_i'(\theta)$ to each site. The value of $\langle X_1 \rangle_\theta$ is taken as the expectation value of the X-measurement on the first site (blue).

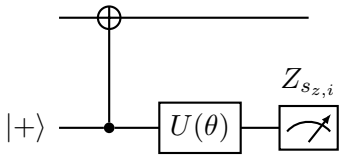

Figure 4.3: Circuit with ancilla for probabilistic implementation of $T_i'(\theta)$ at each site.

To mitigate this, we can pull out cluster state stabilizers from the cluster state and propogate them forwards in time. They flip any relative sign in $T_i'/\bar{T}_i'$, on pairs of the even and odd sub-lattices. That is, a pattern of $\bar{T}_i'$s is correctable if:

$$\sum_{i \text{ even}} s_{z,i} \mod 2 = 0, \quad \sum_{i \text{ odd}} s_{z,i} \mod 2 = 0 \tag{4.5}$$

If this condition is satisfied, then the effect of pulling out the stabilizers is (in each qubit line):

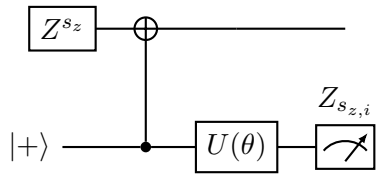

Figure 4.4: Circuit with ancilla for probabilistic implementation of $T_i'(\theta)$ at each site, with correction due to pullout of cluster state stabilizers.

We then observe the phase kickback circuit identity:

$$\Pi_{X_i:s_i} CX_{j,i} = Z^{s_i} j \Pi_{X_i:s_i} \tag{4.6}$$

which is graphically represented in Fig. 4.5.

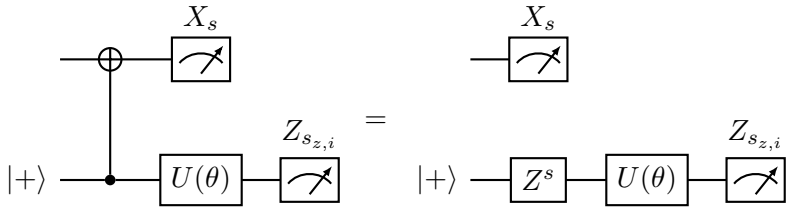

Figure 4.5: Circuit representation of the phase kickback identity Eq. (4.6).

Applying the phase kickback to each qubit line and pushing the $Z^{s_{z,i}}$ correction past the X measurements to yield $s_i \mapsto s_i + s_{z,i} = s_i'$, we get the circuit shown in Fig. 4.6.

This is a major simplification with half of the qubits (the ancillas) disconnecting from the circuit! Looking at the remaining residual circuit, the remaining measurements (excepting two) implement half-teleportations as discussed in Section 2.2.3. This leads to the series of simplifications provided in Fig. 4.7.

The circuit residue therefore finds that $s_1' + s_3' \mod 2 = 0$, $s_2' + s_4' \mod 2 = 0$. Because of the

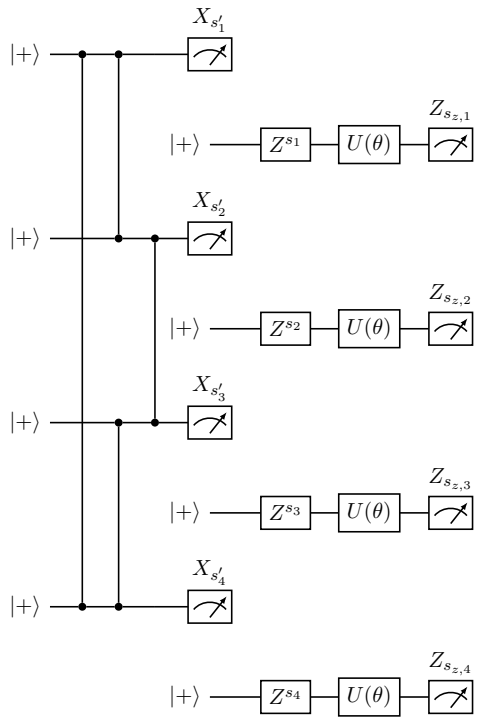

Figure 4.6: Circuit simplification of Fig. 4.2. The ancillas split off from the main circuit due to the phase kickback identity in Eq. (4.6).

$\mathbb{Z}_2 \otimes \mathbb{Z}_2$ symmetry it holds that $\sum_{i \text{ even}} s_i = \sum_{j \text{ odd}} s_j = 0$, and therefore

$$\sum_{i \text{ even}} s'_i \mod 2 = \sum_{i \text{ even}} s_i + s_{z,i} \mod 2 = \sum_{i \text{ even}} s_{z,i} \mod 2,$$

and the same follows for the odd sites. Therefore the circuit residue merely reinforces the post-selection criterion Eq. (4.5) which we already assumed, and therefore does not have to be performed.

We have therefore reduced the original 8-qubit circuit measurement for the local magnetic field for the Ansatz Eq. (4.1) to the repeated running of a 1-qubit circuit. The last step is to transform the 1-qubit circuit (the disconnected ancillas as depicted in Fig. 4.6 which depend on s_z and s separately to those that only depend on $s' = s + s_z$. Since U is real, $[U, Y] = 0$ and so $UZ = ZXUX$. Therefore we perform the last simplification, as displayed in Fig. 4.8. The final circuit is precisely the one used in the algorithm in Table 4.2, thus concluding its derivation.

Before moving on, we note again that originally, the implementation of (non-unitary) $T'(\theta)$ was

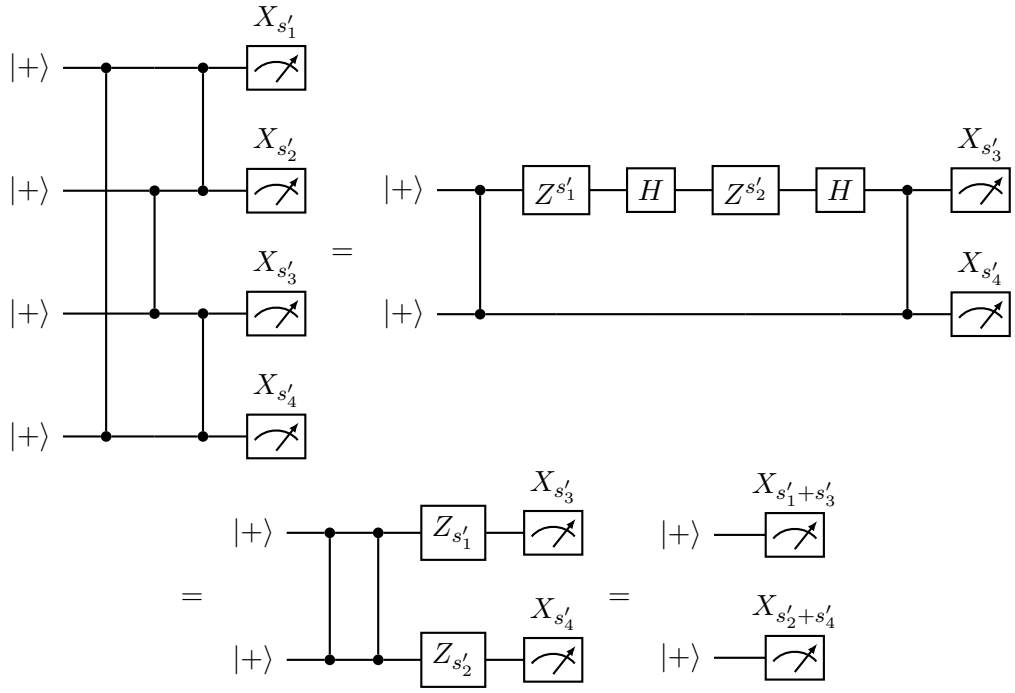

Figure 4.7: Series of circuit simplifications of the residual $\langle X_i \rangle_\theta$ measurement circuit. In the first step we carry out two half-teleportation steps. In the second step we commute the single qubit gates past the CZ. In the final step we use that $(CZ)^2 = I$ and push the Z gates past the measurement, where they flip the measurement outcome. The final circuit is merely a reinforcement of an already assumed post-selection criterion and hence does not have to be executed.

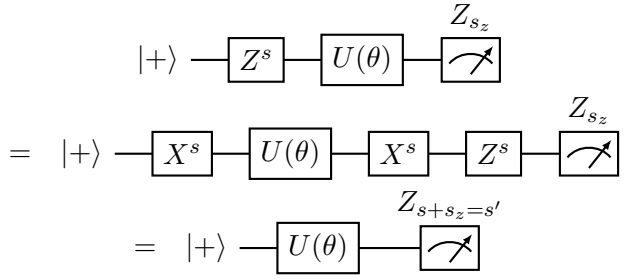

Figure 4.8: Final simplification of the one-qubit ancilla circuits for the $\langle X_i \rangle_\theta$ measurement.

inefficient, and required 8 qubits to make a 4 qubit state. Yet for the choice of final measurement bases of $\langle X_i \rangle_\theta$, the entire circuit simplifies into the repeated running of just a single-qubit circuit. Note that while we showed the $n = 4$ case above, the argument easily generalizes to larger rings, where we still see the drastic simplification of a $2n$-qubit circuit to a single-qubit circuit.

Having discussed a $\langle X_i \rangle_\theta$ measurement algorithm, we now derive an analogous algorithm for the $\langle K_i \rangle_\theta$ (stabilizer) measurement.

4.3 VQE algorithm for $\langle K_i \rangle_\theta$

The protocol for the measurement of $\langle K_i \rangle_\theta$ for a ring of size 4 is described in Table 4.3, with accompanying correctness proof and derivation.

Protocol for the measurement of the cluster stabilizer.

For a ring of size 4, execute the following steps:

1. Run the two one-qubit circuits:

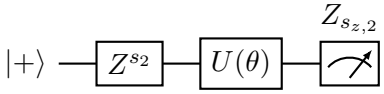

   for a equal number of times for $s_2 = 0$ and $s_2 = 1$ (and a large number of times in total). As before, in the Z-basis, $U \cong \begin{pmatrix} \cos\theta & \sin\theta \\ -\sin\theta & \cos\theta \end{pmatrix}$.

2. For many times, run the (four) three-qubit circuits:

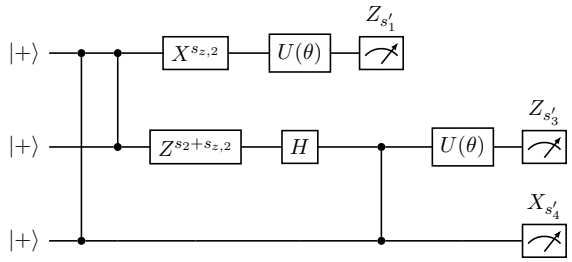

3. Pair up each circuit from step 1 with the circuit with the same corresponding $s_2/s_{z,2}$ values in step 2. If $s'_1 = 1$ or $s'_3 = 1$, discard the pair.

4. For many times, run the following 1-qubit circuit:

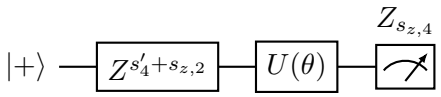

   and pair up these circuits with the step 1/2 pairs with the same corresponding $s'_4/s_{z,2}$ values. If $s_{z,2} + s_{z,4} \mod 2 \neq 0$, then discard the trio.

5. Denote by N_+ the number of surviving batches with $s_2 = 0$ and N_- the number of remaining batches with $s_2 = 1$. Then, calculate $\langle K_i \rangle$ as:

$$\langle K_i \rangle = \frac{N_+ - N_-}{N_+ + N_-}$$

Table 4.3: Procedure for obtaining the expectation value of the cluster stabilizer term for the ansatz state of Eq. (4.1)

Proof of correctness

Like in the case of the magnetic field measurement algorithm, we show the correctness of Table 4.3 by showing that it reproduces the straight quantum mechanical calculation of for the cluster stabilizer expectation value:

$$\langle K_i \rangle_\theta = \langle K_2 \rangle_\theta = \langle \Psi(\theta) | Z_1 X_2 Z_3 I_4 | \Psi(\theta) \rangle = \frac{1-x^2}{1+x^2}. \tag{4.7}$$

where $x = 2\cos\theta\sin\theta$. A derivation of this formula is found in the appendix. Denoting by $p_{s_{z,2}}$ the measurement probabilities for the circuit in Step 1, if $s_2 = 0$ we find:

$$p_{s_{z,2}}(0) = \frac{1+x}{2}, \quad p_{s_{z,2}}(1) = \frac{1-x}{2}$$

and if $s_2 = 1$ the above probabilities are exchanged. Case-by-case analysis of the circuit in Step 2 shows that $p_{s'_1}(0) = \frac{1}{2}$ for all values of s_2 and that $p_{s'_3}(0) = 1$ if $s_2 = 0$ and $p_{s'_3}(0) = x^2$ if $s_2 = 1$. Further, we find that $s'_4 + s_{2,z} = 0$ if $s_2 = 0$ and $s'_4 + s_{2,z} = 1$ if $s_1 =$ and hence for the circuit in Step 3 we inherit the probabilities from the circuit in step 1. All in all, if $s_2 = 0$ the batch has survival probability:

$$p_{++} = p_{s_{z,2}}(0)p_{s'_1}(0)p_{s'_3}(0)p_{s_{z,4}}(0) + p_{s_{z,2}}(1)p_{s'_1}(0)p_{s'_3}(0)p_{s_{z,4}}(1) = \frac{1+x^2}{4}$$

Analogously, if $s_2 = 1$ the batch has survival probability:

$$p_{--} = p_{s_{z,2}}(0)p_{s'_1}(0)p_{s'_3}(0)p_{s_{z,4}}(0) + p_{s_{z,2}}(1)p_{s'_1}(0)p_{s'_3}(0)p_{s_{z,4}}(1) = x^2\frac{1+x^2}{4} = x^2 p_{++}$$

Therefore calculating $\langle K_i \rangle$ we find:

$$\langle K_i \rangle = \frac{p_{++} - p_{--}}{p_{++} + p_{--}} = \frac{p_{++} - x^2 p_{++}}{p_{++} + x^2 p_{++}} = \frac{1-x^2}{1+x^2}.$$

This agrees with the quantum-mechanical value of Eq. (4.7).

Circuit derivation

The straightforward state for measuring the cluster term on the ansatz state Eq. (4.1) is:

Where $\langle K_2 \rangle$ is calculated as $\langle (-1)^{s_1+s_2+s_3} \rangle$. We have the same correctability condition as in

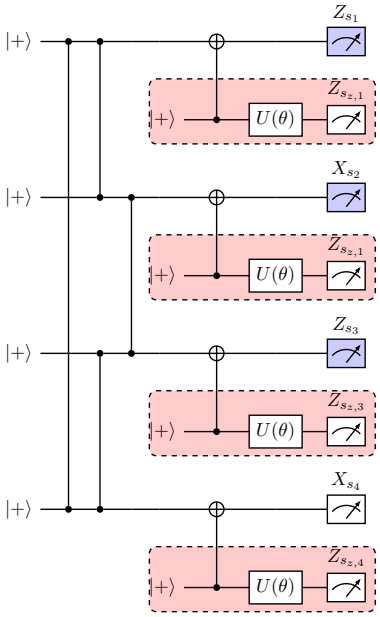

Figure 4.9: Unsimplified circuit for measurement of the expectation value $\langle K_2 \rangle_\theta$ for the VQE algorithm. The ancilla measurements (red) correspond to the probabilistic application of $T_i'(\theta)$ to each site. The value of $\langle K_2 \rangle_\theta$ is taken as $\langle (-1)^{s_1+s_2+s_3} \rangle$ (blue).

the $\langle X_i \rangle$ algorithm, with:

$$\sum_{i\text{even}} s_{z,i} \mod 2 = 0, \quad \sum_{i\text{odd}} s_{z,i} \mod 2 = 0 \tag{4.8}$$

and assuming this condition is satisfied, the effect of pulling out the stabilizers in each qubit line is given by the circuit in Fig. 4.10. Note that unlike the $\langle X_i \rangle$ case, the X part of the stabilizer on the second qubit flips the measurement outcome on the first qubit (in the previous protocol, the X commuted past the X_{s_1} measurement and could be ignored). We again use the phase kickback identity as in Eq. (4.6) that:

$$\Pi_{X_i:s_i} CX_{j,i} = Z^{s_i} j \Pi_{X_i:s_i}$$

as well as that $H^2 = I$ to obtain the circuit in Fig. 4.11.

Next, we conjugate $HXH = Z$ and push the remaining H past the Z_{s_1}/Z_{s_3}-measurements to convert them to X_{s_1}/X_{s_3}-measurements. We also push the $Z^{s_{z,2}}/Z^{s_{z,4}}$ gates past the X_{s_2}/X_{s_4}

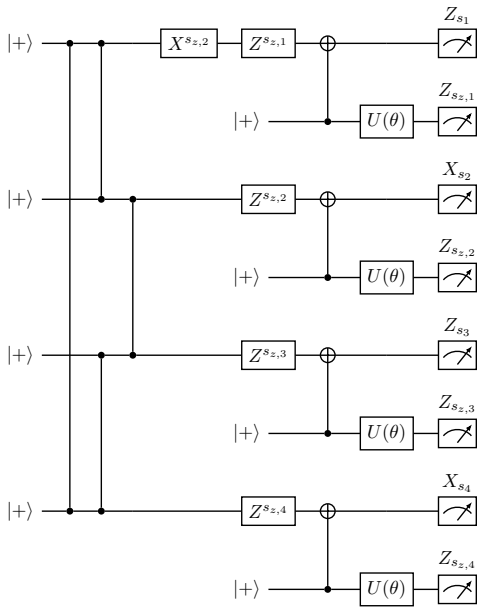

Figure 4.10: Circuit for measurement of $\langle K_2 \rangle_\theta$, with cluster state stabilizer pullout corrections to probabilistic implementations of per-site $T_i'(\theta)$.

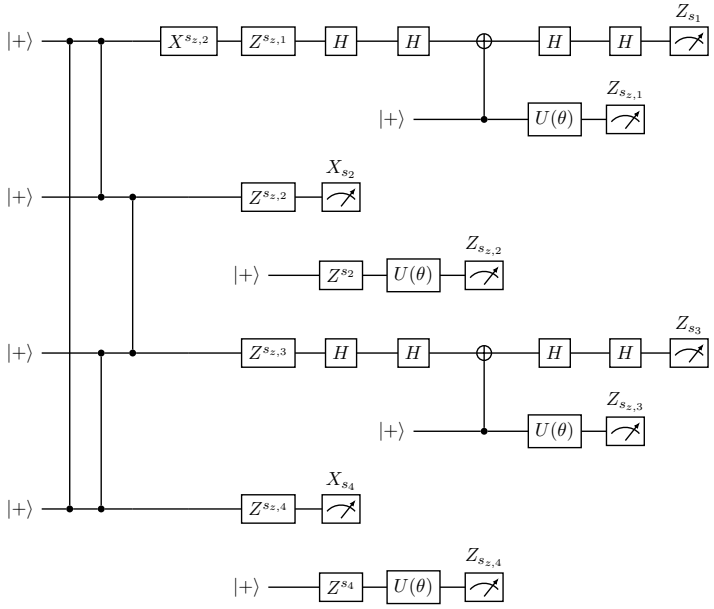

Figure 4.11: Equivalent circuit to Fig. 4.10 obtained by application of phase kickback identity and $H^2 = I$. We note the ancillas for qubits 2/4 split off from the main circuit.

measurements, defining $s'_i = s_i + s_{z,i}$ as the new measurement outcomes. Finally, we commute some of the initial CZ gates to setup for a half-teleportation. These identities yield the circuit in Fig. 4.12.

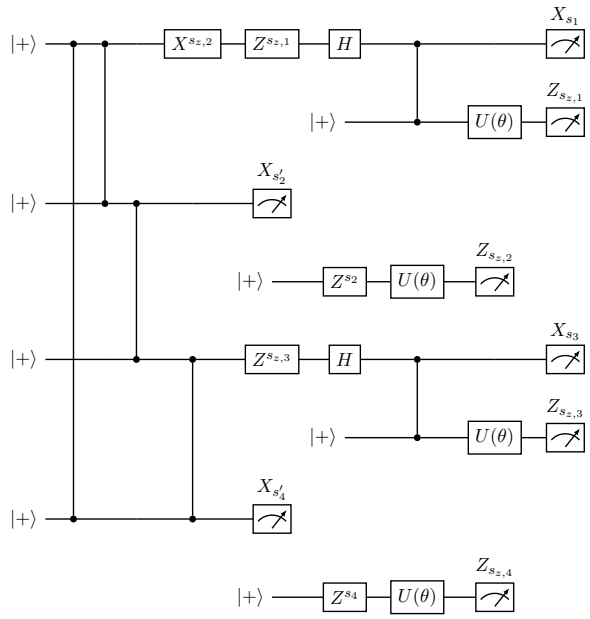

Figure 4.12: Equivalent Circuit to Fig. 4.11 obtained by Hadamard conjugations and moving gates past measurements.

Now we observe three locations where we may invoke a half-teleportation, namely between qubits 2/3 and between the qubit and ancilla for qubits 1 and 3. Carrying out these half-teleportations, we obtain the circuit in Fig. 4.13.

Now, we observe the problem that the circuit above seems unexecutable. In particular, there appears to be gates $Z^{s_{z,1}}$ and $Z^{s_{z,3}}$ that are conditioned on the outcome of a future measurement. To resolve this, we introduce a new post-selection condition of $s_{z,1} = s_1$ and $s_{z,3} = s_3$. Combining this new condition with the with the conjugation identity $HZH = X$ and the fact that $ZX \propto Y$, we obtain the circuit in Fig. 4.14.

Since U is real, $[Y, U] = 0$ and we can commute Y^{s_i} past U. Further, we can push Y^{s_i} past the Z-measurement, flipping the outcome of the measurement. This yields the final circuit in Fig. 4.15.

But note that the condition $s_{z,1} = s_1$ and $s_{z,3} = s_3$ implies $s'_1 = s'_3 = 0$ and this forms the two post-selection conditions given in Step 2 of the Protocol. Furthermore, the odd-site correctability

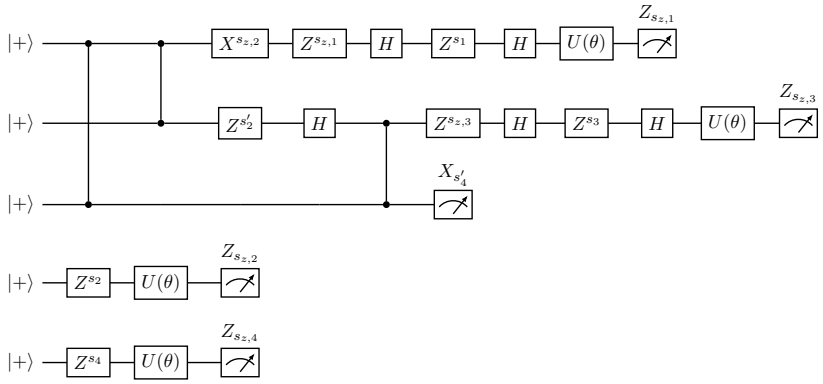

Figure 4.13: Equivalent Circuit to Fig. 4.12 obtained by three half-teleportation steps.

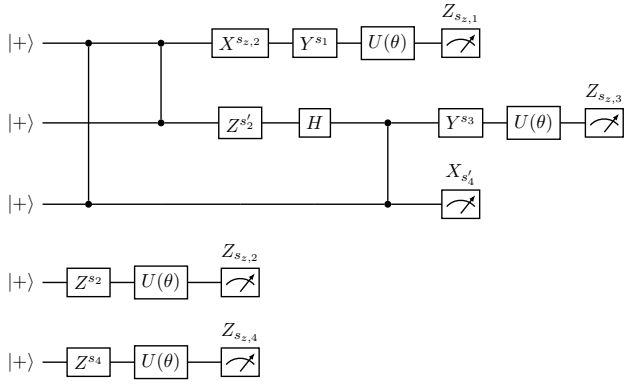

Figure 4.14: Simplification of Circuit in Fig. 4.12 obtained by the introduction of a new post-selection condition of $s_{z,1} = s_1$ and $s_{z,3} = s_3$.

conditions (4.8) imply that $s_{z,1} = s_{z,3}$ and so $s_1 = s_3$; hence the sign of s_2 alone determines the sign of K_2 (as $K_2 = (-1)^{s_1+s_2+s_3}$), with $s_2 = 0$ corresponding to $K_i = +1$ and $s_2 = 1$ corresponding to $K_i = -1$. Finally, the even-site correctability conditions imply $s_{z,2} = s_{z,4}$ and hence $s_4 = s_4 + s_{z,4} + s_{z,2} = s'_4 + s_{z,2}$ which gives the circuit and post-selection condition in step 3 of the protocol. This concludes the circuit derivation of the algorithm.

We again remark that as in the case with the $\langle X_i \rangle$ measurement circuits, we have a tremendous amount of circuit simplification; the originally 8 qubit circuit has reduced to a 3 qubit circuit. Although out of the scope of this thesis, we again note that even for larger ring sizes similar simplifications are seen, with an arbitrarily large ring collapsing down to a constant 4-qubit circuit when the cluster stabilizer K_i is measured. Though the non-unitarity of $T'(\theta)$ makes the general

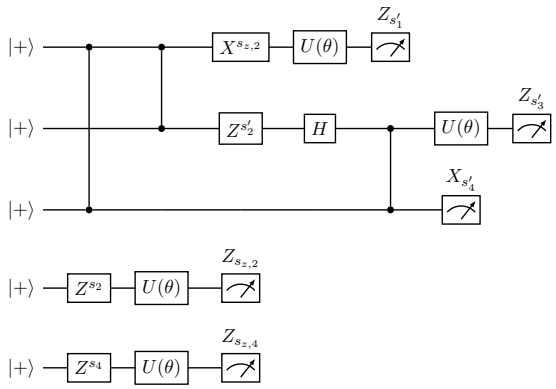

Figure 4.15: Fully simplified circuit for the $\langle K_2 \rangle_\theta$ measurement, as obtained by commuting the Y^{s_i} gates past U and the Z-measurements in the circuit in Fig. 4.14.

creation of the states $T'(\theta)|C\rangle$ inefficient, we see cascading simplification for certain choices of measurement sequences.

A small note on the physical execution of the algorithm: the circuits in Step 2 are unoptimal for performing on the IBM circuit architectures, which do not contain a 3-ring. This is resolved efficiently via the circuit identity in Fig. 4.16.

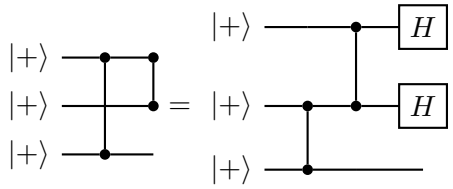

Figure 4.16: A cluster state identity. We can invoke the above identity in the execution of the algorithm provided in Table 4.3 to circumvent the lack of a 3-qubit ring in the IBM architecture (as given in Fig. 3.4).

Chapter 5

Results - Experiments

5.1 Rotation-counter rotation experimental result

The protocol for the rotation-counter rotation algorithm as described in Table 4.1 was programmed in Qiskit and performed in a quantum circuit simulator. The coefficients for $T(\alpha)$ required for the algorithm were found via a classical variational algorithm. The results are provided in Fig. 5.1, with each point corresponding to a single run of the described algorithm at a given α.

We observe that when performed on a quantum circuit simulator, the algorithm produces the theory result exactly, up to statistical fluctuations arising from the probabilistic nature of measurement. This verifies the correctness of the algorithm. Next, the algorithm/circuits were performed on the 5-qubit *ibmq_manila* quantum device The results are shown in Fig. 5.2 below.

We observe that the value of $\langle \overline{X} \rangle$ is here consistently lower than the numerical prediction due to the effects of measurement, gate, and decoherence errors present in the physical quantum device. However, we note that the overall characteristic shape of the $\langle \overline{X} \rangle$ curve from the numerical prediction is reflected in the experiment. We will now proceed to obtain these results in a more quantum mechanical fashion; namely by obtaining $T(\alpha)$ using VQE methods.

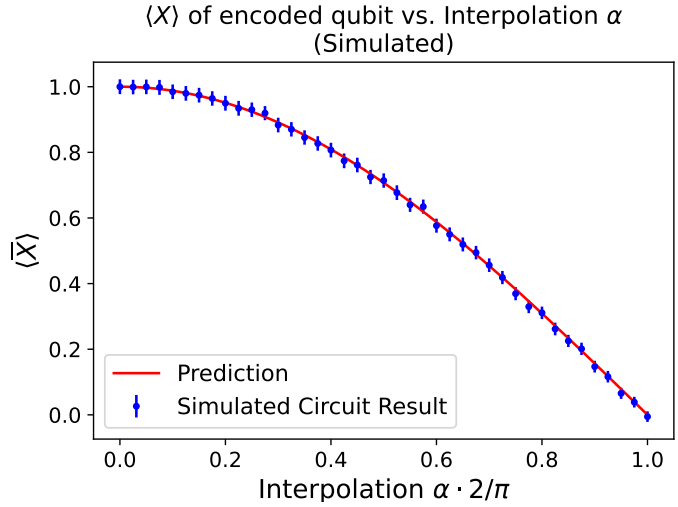

Figure 5.1: $\langle \overline{X} \rangle$ vs. interpolation parameter α for the 4-ring rotation-counter rotation protocol. The algorithm in Table 4.1 was executed on a classical computer, using the noiseless Qiskit qasm circuit simulator. Each circuit in the algorithm was run for 8000 shots. Error bars represent 2 standard errors of the mean. $T(\alpha)$ was obtained via classical optimization. The prediction curve is from Fig 2.12.

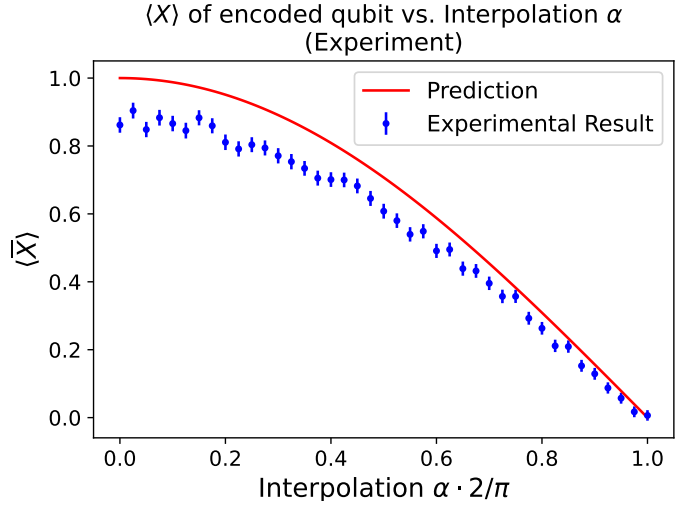

Figure 5.2: $\langle \overline{X} \rangle$ vs. interpolation parameter α for the 4-ring rotation-counter rotation protocol. The algorithm in Table 4.1 was executed on the *ibmq_manila* quantum device. Each circuit in the algorithm was run for 8000 shots. Error bars represent 2 standard errors of the mean. Standard measurement error mitigation procedures as provided by Qiskit were applied. $T(\alpha)$ was obtained via classical optimization. The prediction curve is from Fig 2.12.

5.2 VQE experimental results

Having provided algorithms for the measurement of $\langle X_i \rangle_\theta$ and $\langle K_i \rangle_\theta$ in Tables 4.2 and 4.3, we now execute these protocols experimentally. The results are provided in Fig. 5.3 below.

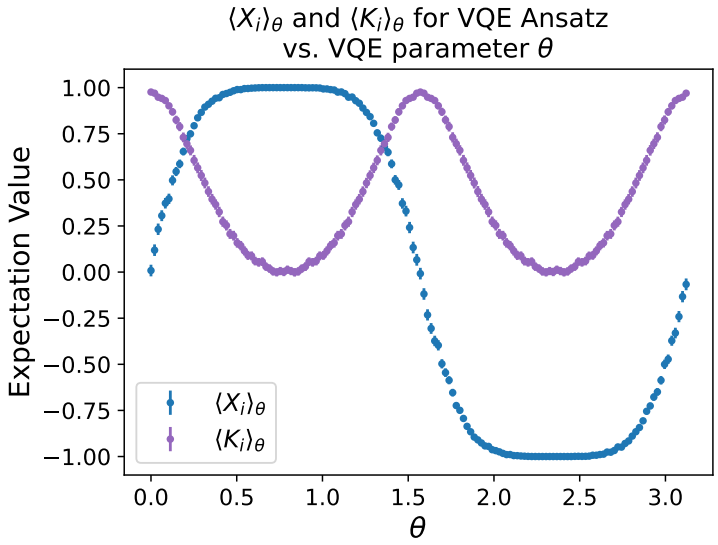

Figure 5.3: Local magnetic field expectation $\langle X_i \rangle_\theta$ and Cluster Stabilizer expectation $\langle K_i \rangle_\theta$ as a function of variational parameter θ as produced by the protocol in Tables 4.2/4.3 for Ansatz state (4.1). The protocols was executed on the *ibmq_manila* quantum device. Each circuit in the protocols was run for 8000 shots. Error bars represent 2 standard errors of the mean. Standard measurement error mitigation procedures as provided by Qiskit were applied.

Now, to find coefficients $a(\alpha), b(\alpha)$ in $T(\alpha) = \bigotimes_i T_i(\alpha) = \bigotimes_i a(\alpha) I_i + b(\alpha) X_i$, we can sweep over the range $0 \leq \theta \leq \pi/4$ (with $\theta = 0$ corresponding to the cluster state and $\theta = \pi/4$ corresponding to the product state) and find what minimizes:

$$E_i = -\cos(\alpha) \langle K_i \rangle_\theta - \sin(\alpha) \langle X_i \rangle_\theta .$$

We then can take $a(\alpha) = \cos(\theta_{\min})), b(\alpha) = \sin(\theta_{\min})$. However, a naive application of this procedure is suceptible to experimental noise in the measurements of $\langle X_i \rangle_\theta$ and $\langle K_i \rangle_\theta$. To avoid this, we first fit the $\langle X_i \rangle_\theta$ and $\langle K_i \rangle_\theta$ data via Fourier series, making use of the periodic structure of the

two expectation values. The Fourier coefficients were solved for as:

$$c_n = \frac{1}{\pi} \sum_{j=1}^{N} \frac{\pi}{N} \langle X_1 \rangle_{\theta_j} \exp(-i2n\theta_j) \tag{5.1}$$

where N is the number of points and $\theta_1, \ldots \theta_N$ were the θs that were sampled in the VQE algorithm. The Fourier sum is then given by:

$$\langle \tilde{X}_1 \rangle(\theta) = \sum_{n=1}^{M} c_n e^{i2n\theta}. \tag{5.2}$$

and analogous relations follow for $\langle K_i \rangle$. Calculating the magnitudes of the coefficients, we find that for $\langle X_i \rangle_\theta$ only the $n = 1, 3, 5$ coefficients are significant, and for $\langle K_i \rangle_\theta$ that only the $n = 0, 2, 4, 6$ coefficients are significant. We discard higher terms of the sum as they would contribute experimental noise. We can then plot the experimental data along with their Fourier sums, as well as the analytical values for $\langle X_i \rangle_\theta$ and $\langle K_i \rangle_\theta$ as given by Eqs. (4.3) and (4.7). This yields Fig. 5.4.

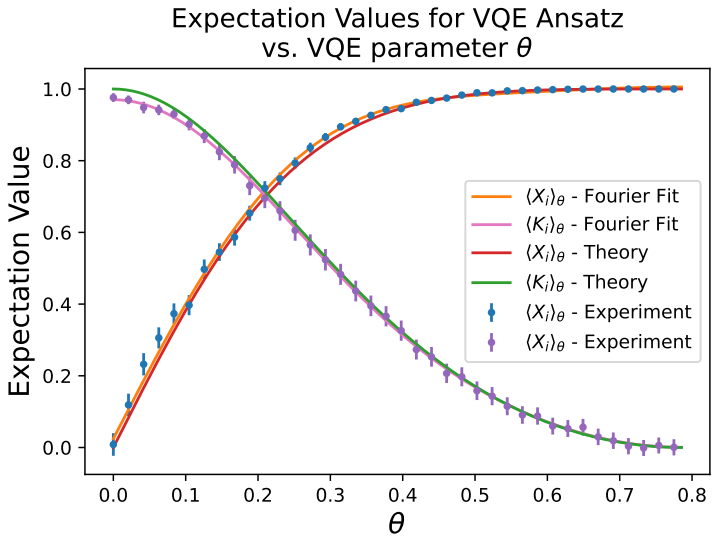

Figure 5.4: Expectation Values for $\langle X_i \rangle_\theta$ and $\langle K_i \rangle_\theta$ for the Ansatz state (4.1). Here the analytical theory value is compared against the experimental results of Fig. 5.3, along with Fourier series fits to the experimental data. Agreement is shown between the Fourier fit and the theory prediction, with the noise from the experimental data being filtered out through the fit.

We can now proceed with the minimization procedure on the Fourier fit functions for $\langle X_i \rangle_\theta$ and $\langle K_i \rangle_\theta$ to find the coefficients $a(\alpha)$ and $b(\alpha)$ of $T(\alpha)$. This yields Fig. 5.5.

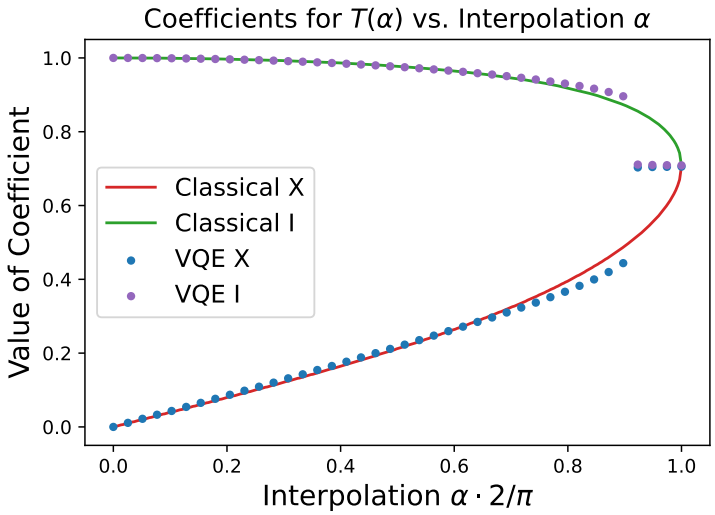

Figure 5.5: Plot of X and I coefficients for transformation operator $T(\alpha)$ as obtained from classical optimization and from VQE data with Fourier series fitting.

We note the fantastic agreement between the coefficients obtained classically and quantum mechanically in the "cluster phase" region of $0 \leq \alpha \leq \pi/4$. However, we note that the VQE result is less successful near the product state, in particular exhibiting a discontinuous jump. The reason for this can be observed in Fig. 5.4, where we see that the value of $\langle X_i \rangle_\theta$ exhibits a plateau close to $\theta = \pi/4$. Since E_i is dominated by $\langle X_i \rangle_\theta$ for α near $\pi/2$, it follows that E_i has a similar plateau in its minima. Small deviations resulting from experimental noise hence have a large effect in this flat region, leading to identical values of θ (and hence identical coefficients for $T(\alpha)$) being chosen in the energy minimization after a certain threshold α close enough to $\pi/2$.

Having found the coefficients for the $T(\alpha)$ operator quantum mechanically, we can repeat the experiments conducted earlier in this section using this new version of the operator.

5.3 Rotation-counter rotation experimental result, with VQE coefficients

The protocol for the rotation-counter rotation algorithm as described in Table 4.1 was performed experimentally, now using the coefficients for $T(\alpha)$ found in the VQE as displayed in Fig. 5.5. The

results are provided in Fig. 5.6 below.

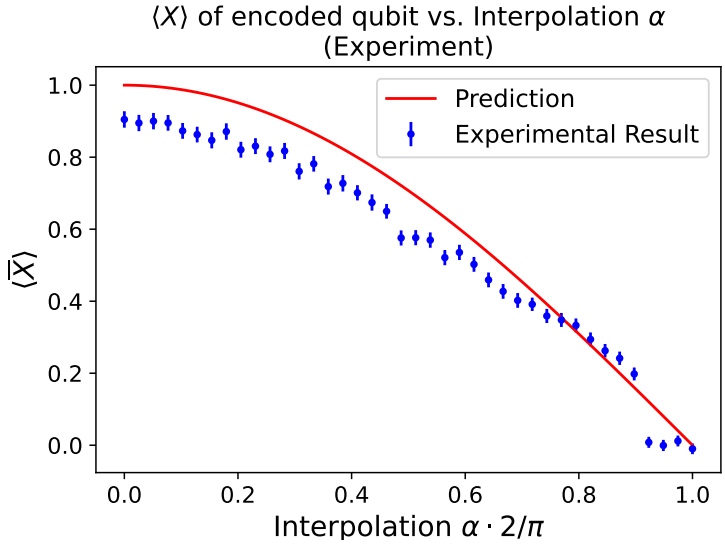

Figure 5.6: $\langle \overline{X} \rangle$ vs. interpolation parameter α for the 4-ring rotation-counter rotation protocol. The algorithm was executed on the *ibmq_manila* quantum device. Each circuit in the algorithm was run for 8000 shots. Error bars represent 2 standard errors of the mean. Standard measurement error mitigation procedures as provided by Qiskit were applied. $T(\alpha)$ was obtained via a VQE optimization algorithm. The prediction curve is from Fig 2.12.

As before, we note the deviations from the numerical prediction result due to loss of fidelity that is unavoidable in physical devices. We further note that due to the VQE optimization having trouble near the product state that the characteristic shape of the curve breaks down in this region (most notably with a jump to zero at $\alpha \sim 9\pi/20$. However, overall (and particularly in the regime of interest in terms of computational power of $0 \leq \alpha \leq \pi/4$) that the experimental result shows good agreement with the predicted characteristic shape of the $\langle \overline{X} \rangle$ curve. We have now completed a genuinely quantum-mechanical run of the counter-rotation experiment, both finding $T(\alpha)$ on a quantum device and executing the experiments to measure $\langle \overline{X} \rangle$ on quantum devices.

Chapter 6

Conclusion & Outlook

In this thesis, we have developed algorithms for the reproduction of a simple protocol to test MBQC computational power in an experimental setting. We have developed a VQE protocol that allows us to obtain arbitrary states in the cluster phase starting from the cluster state. We have also developed a protocol that allows us to run the rotation-counter rotation test of computational power of these ground states. We have run these 4-qubit protocols experimentally on IBM NISQ devices, and while experimental noise in general causes a reduction in fidelity as well as differing behavior near the product state, we find that the characteristics of the theoretical predictions are preserved in the experimental results.

Our results serve as a first experimental demonstration of the robustness of computational power of MBQC resource states. Previous theory work predicts that computational power is not a property of a specific state (such as the cluster state) and that states away from the cluster state can possess the capability for computation; both in the infinite case where computational power is a property of an entire phase of matter, and the finite case where computational power can be characterized by a string order parameter. Our experimental results are consistent with predictions in the finite regime. We also demonstrate, through this work, the viability for NISQ-era devices to showcase phenomenology concerning computational resources, and open up the possibility for future experiments in this vein.

An immediate next step in these results is to resolve the behaviour near the product state (α close to $\pi/2$) which can likely be accomplished with pre-processing or averaging of the experimental data. Resolving this, there are two major possible directions for this work. The first is an extension to larger system sizes, where not only can we observe effects of decoherence when doing MBQC with resource states away from the cluster state, but we can experimentally demonstrate techniques for

managing such decoherence. The techniques built up in this thesis are conducive for the showcase of the "divide-and-conquer" strategy of minimizing decoherence through splitting of the rotation angle in symmetry-breaking measurements. The experimental demonstration of the "counter-intuitive regime" of splitting rotations as much as possible is also of interest to pursue, but requires a more sophisticated VQE ansatz than the one provided in this work. The "counter-intuitive regime" concerns the interplay of correlation length and splitting of rotations, and there requires an ansatz state with a length scale. Our current ansatz is local and contains no such length scale, and further developments are required in this area to build towards an experimental demonstration. The second direction comes out of the circuit simplification results we observe in the VQE algorithms. Through these algorithms we observe a drastic simplification of large, system-size dependent circuits to small, constant-qubit overhead circuits as a consequence of the choice of the prepared state and measurement bases. It may be possible that this result is indicative of some underlying structure that allows for more general circuit simplification; thus opening the way for potential projects in the line of quantum compilation and quantum programming languages.

Bibliography

[1] I. M. Georgescu, S. Ashhab, and Franco Nori. Quantum simulation. *Rev. Mod. Phys.*, 86:153–185, Mar 2014. → page 1

[2] Richard P. Feynman. Simulating physics with computers. *International Journal of Theoretical Physics*, 21(6/7), 1982. → page 1

[3] Peter W. Shor. Polynomial-time algorithms for prime factorization and discrete logarithms on a quantum computer. *SIAM Journal on Scientific and Statistical Computing*, 26(5):1484–1509, 1997. → pages 1, 8

[4] Lov K. Grover. A fast quantum mechanical algorithm for database search. In *Proceedings, 28th Annual ACM Symposium on the Theory of Computing*, 1996. → page 1

[5] Aram W. Harrow, Avinatan Hassidim, and Seth Lloyd. Quantum algorithm for linear systems of equations. *Physical Review Letters*, 103(15), oct 2009. → page 1

[6] John Preskill. Quantum computing in the nisq era and beyond. *Quantum*, 2:79, 2018. → page 1

[7] Frank Arute, Kunal Arya, Ryan Babbush, Dave Bacon, Joseph Bardin, Rami Barends, Rupak Biswas, Sergio Boixo, Fernando Brandao, David Buell, Brian Burkett, Yu Chen, Jimmy Chen, Ben Chiaro, Roberto Collins, William Courtney, Andrew Dunsworth, Edward Farhi, Brooks Foxen, Austin Fowler, Craig Michael Gidney, Marissa Giustina, Rob Graff, Keith Guerin, Steve Habegger, Matthew Harrigan, Michael Hartmann, Alan Ho, Markus Rudolf Hoffmann, Trent Huang, Travis Humble, Sergei Isakov, Evan Jeffrey, Zhang Jiang, Dvir Kafri, Kostyantyn Kechedzhi, Julian Kelly, Paul Klimov, Sergey Knysh, Alexander Korotkov, Fedor Kostritsa, Dave Landhuis, Mike Lindmark, Erik Lucero, Dmitry Lyakh, Salvatore Mandrà, Jarrod Ryan McClean, Matthew McEwen, Anthony Megrant, Xiao Mi, Kristel Michielsen, Masoud Mohseni, Josh Mutus, Ofer Naaman, Matthew Neeley, Charles Neill, Murphy Yuezhen Niu, Eric Ostby, Andre Petukhov, John Platt, Chris Quintana, Eleanor G. Rieffel, Pedram Roushan, Nicholas Rubin, Daniel Sank, Kevin J. Satzinger, Vadim Smelyanskiy, Kevin Jeffery Sung, Matt Trevithick, Amit Vainsencher, Benjamin Villalonga, Ted White, Z. Jamie Yao, Ping Yeh, Adam Zalcman, Hartmut Neven,

and John Martinis. Quantum supremacy using a programmable superconducting processor. *Nature*, 574:505–510, 2019. → page 1

[8] Feng Pan, Keyang Chen, and Pan Zhang. Solving the sampling problem of the sycamore quantum supremacy circuits, 2021. → page 1

[9] Daniel Gottesman. The heisenberg representation of quantum computers. 6 1998. → pages 1, 8

[10] D. Gross, S. T. Flammia, and J. Eisert. Most quantum states are too entangled to be useful as computational resources. *Physical Review Letters*, 102(19), May 2009. → pages 1, 8

[11] Peter W. Shor. Why haven't more quantum algorithms been found? *Journal of the ACM*, 50(1):87–90, 2003. → page 1

[12] Robert Raussendorf and Hans J. Briegel. A one-way quantum computer. *Physical Review Letters*, 86(22), 2001. → pages 2, 8, 16

[13] Dominic V. Else, Ilai Schwarz, Stephen D. Bartlett, and Andrew C. Doherty. Symmetry-protected phases for measurement-based quantum computation. *Physical Review Letters*, 108(24), Jun 2012. → pages 2, 18, 20

[14] Robert Raussendorf, Dong-Sheng Wang, Abhishodh Prakash, Tzu-Chieh Wei, and David T. Stephen. Symmetry-protected topological phases with uniform computational power in one dimension. *Physical Review A*, 96(1), Jul 2017. → pages 2, 18, 19, 20

[15] Arnab Adhikary. Symmetry protected measurement-based quantum computation in finite spin chains. Msc, University of British Columbia, 2021. → pages 2, 10, 19, 21

[16] Henry Maurice Sheffer. A set of five independent postulates for boolean algebras, with application to logical constants. *Transactions of the American Mathematical Society*, 14(4):481–488, 1913. → page 7

[17] Michael A. Nielsen and Isaac L. Chuang. *Quantum Computation and Quantum Information*. Cambridge University Press, 2000. → page 7

[18] Charles H. Bennett, Gilles Brassard, Claude Crépeau, Richard Jozsa, Asher Peres, and William K. Wootters. Teleporting an unknown quantum state via dual classical and einstein-podolsky-rosen channels. *Phys. Rev. Lett.*, 70:1895–1899, Mar 1993. → page 11

[19] Subir Sachdev. *Quantum Phase Transitions*. Cambridge University Press, 2 edition, 2011. → page 17

[20] Lev Davidovich Landau. On the theory of phase transitions. I. *Phys. Z. Sowjet.*, 11:26, 1937. → page 17

[21] D. C. Tsui, H. L. Stormer, and A. C. Gossard. Two-dimensional magnetotransport in the extreme quantum limit. *Phys. Rev. Lett.*, 48:1559–1562, May 1982. → page 17

[22] Xiao-Gang Wen. Topological orders and edge excitations in fractional quantum hall states. *Advances in Physics*, 44(5):405–473, Oct 1995. → page 17

[23] Matthew Fishman, Steven R. White, and E. Miles Stoudenmire. The itensor software library for tensor network calculations. *CoRR*, abs/2007.14822, 2020. → page 22

[24] Mario Motta and Julia Rice. Emerging quantum computing algorithms for quantum chemistry, 2021. → page 27

[25] IBM Quantum. Services, 2021. → page 28

[26] M. Hein, J. Eisert, and H. J. Briegel. Multiparty entanglement in graph states. *Physical Review A*, 69(6), Jun 2004. → page 32

Appendix A

Derivation of $\langle X_\mathrm{i} \rangle$ and $\langle K_\mathrm{i} \rangle$ for VQE Ansatz

In this appendix, we derive the expectation values $\langle X_\mathrm{i} \rangle_\theta$ and $\langle K_\mathrm{i} \rangle_\theta$ for the VQE ansatz:

$$|\Psi(\theta)\rangle = T'(\theta)|C\rangle = \left(\bigotimes_{i=1}^{N} \cos(\theta) I_i + \sin(\theta) X_i \right) |C\rangle \tag{A.1}$$

where $|C\rangle$ is a cluster ring of size $N = 2n$ for integer $n > 1$.

First, we observe that $|C\rangle$ is a stabilizer state in a Hilbert space with dimension 2^{2n}, and with a stabilizer group S generated by Pauli observables $\{Z_{i-1} X_i Z_{i+1}\}_{i=1}^{2n}$. We can therefore write the density operator corresponding to $|C\rangle$ as:

$$\rho_C = |C\rangle\langle C| = \frac{1}{2^{2n}} \sum_{g \in S} g \tag{A.2}$$

Where the gs are products of the stabilizer generators $Z_{i-1} X_i Z_{i+1}$. We may then write the density operator corresponding to $|\Psi(\theta)\rangle$ as:

$$\rho_\theta = T'(\theta)|C\rangle\langle C|T'^\dagger(\theta) = T'(\theta)\rho_C T^\dagger(\theta) \tag{A.3}$$

where in the last equality we note that the coefficients of $T'(\theta)$ are all real and hence $T'^\dagger(\theta) = T'(\theta)$. We note ρ_θ is not a normalized density operator due to the non-unitarity of $T'(\theta)$, but we can nevertheless do calculations with it so long as we include a normalization factor. In particular for the operators of interest, we have:

$$\langle X_i \rangle_\theta = \langle X_1 \rangle_\theta = \frac{\mathrm{Tr}(\rho_\theta X_1)}{\mathrm{Tr}(\rho_\theta)} \tag{A.4}$$

$$\langle K_i \rangle_\theta = \langle Z_1 X_2 Z_3 \rangle_\theta = \frac{\mathrm{Tr}(\rho_\theta Z_1 X_2 Z_3)}{\mathrm{Tr}(\rho_\theta)}. \tag{A.5}$$

where in the first equality of each line we use the translation invariance of $|\Psi(\theta)\rangle$ (and so we may without loss of generality choose X_1 and $Z_1 X_2 Z_3$).

We first calculate $\mathrm{Tr}(\rho_\theta)$. By the cyclicity of the trace, we have:

$$\mathrm{Tr}(\rho_\theta) = \mathrm{Tr}(T'(\theta)\rho_C T'(\theta)) = \mathrm{Tr}(T'^2(\theta)\rho_C)$$

Calculating $T'^2(\theta)$ we find:

$$T'^2(\theta) = \bigotimes_{i=1}^{2n} \left((\cos^2\theta + \sin^2\theta) I_i + (2\cos\theta\sin\theta) X_i \right) = \bigotimes_{i=1}^{2n} (I_i + x X_i)$$

where we define $x = 2\cos\theta\sin\theta$ in the last equality. In considering the trace of $T'^2(\theta)\rho_C$, we consider that only the terms proportional to the identity will contribute (as any terms containing Pauli Z or X operators will be traceless). Since $T'^2(\theta)$ only contains identity and Pauli-X operators, all stabilizers in the sum of Eq. A.2 with Pauli-Zs will vanish (as they cannot be "cancelled out" by $T'2$). The only terms in the sum over cluster state stabilizers in ρ_C that do not contain pauli-Z terms are $\bigotimes_{i=1}^n I_i$, $\bigotimes_{i=1}^n X_i$, $I_1 X_2 \ldots I_{2n-1} X_{2n}$, and $X_1 I_2 \ldots X_{2n-1} I_{2n}$. When multiplying by $T'^2(\theta)$, each of these four stabilizers yields a single identity term that contributes to the trace, namely:

$$\mathrm{Tr}(T'^2(\theta) \bigotimes_{i=1}^{n} I_i) = 2^{2n}$$

$$\mathrm{Tr}(T'^2(\theta) \bigotimes_{i=1}^{n} X_i) = 2^{2n} x^{2n}$$

$$\mathrm{Tr}(T'^2(\theta) I_1 X_2 \ldots I_{2n-1} X_{2n}) = \mathrm{Tr}(T'^2(\theta) X_1 I_2 \ldots X_{2n-1} I_{2n}) = 2^{2n} x^n$$

Therefore:

$$\mathrm{Tr}(\rho_\theta) = \mathrm{Tr}\left(T'^2(\theta) \left(\frac{1}{2^{2n}} \sum_{g \in S} g \right) \right) = 1 + 2x^n + x^{2n} = (1 + x^n)^2 \tag{A.6}$$

Next, we calculate $\mathrm{Tr}(\rho_\theta X_1)$. Since $T'(\theta)$ consists solely of identities and Pauli-X operators, it commutes with X_1 and hence:

$$\mathrm{Tr}(\rho_\theta X_1) = \mathrm{Tr}(T'(\theta)\rho_C T'(\theta) X_1) = \mathrm{Tr}(T'(\theta)\rho_C X_1 T'(\theta)) = \mathrm{Tr}(T'^2(\theta)\rho_C X_1)$$

where in the last equality we again use cyclicity. Again since only terms proportional to the identity contribute, we can ignore all terms in $\rho_C X_1$ that contain Pauli-Z terms. The remaining four terms that consist solely of identies and Pauli-Xs are $X_1 \cdot \bigotimes_{i=1}^n I_i$, $X_1 \cdot \bigotimes_{i=1}^n X_i$, $X_1 \cdot (I_1 X_2 \dots I_{2n-1} X_{2n})$, and $X_1 \cdot (X_1 I_2 \dots X_{2n-1} I_{2n})$. When multiplying by $T'^2(\theta)$, each of these four stabilizers yields a single identity term that contributes to the trace, namely:

$$\begin{aligned}
\mathrm{Tr}(T'^2(\theta) X_1 \cdot \bigotimes_{i=1}^n I_i) &= 2^{2n} x \\
\mathrm{Tr}(T'^2(\theta) X_1 \cdot \bigotimes_{i=1}^n X_i) &= 2^{2n} x^{2n-1} \\
\mathrm{Tr}(T'^2(\theta) X_1 \cdot (I_1 X_2 \dots I_{2n-1} X_{2n})) &= 2^{2n} x^{n+1} \\
\mathrm{Tr}(T'^2(\theta) X_1 \cdot (X_1 I_2 \dots X_{2n-1} I_{2n})) &= 2^{2n} x^{n-1}
\end{aligned}$$

Therefore:

$$\mathrm{Tr}(\rho_\theta X_1) = \mathrm{Tr}\left(T'^2(\theta) \left(\frac{1}{2^{2n}} \sum_{g \in S} g \right) X_1 \right) = x + x^{n-1} + x^{n+1} + x^{2n-1} = x(1+x^{n-2})(1+x^n) \quad \text{(A.7)}$$

Finally, we calculate $\mathrm{Tr}(\rho_\theta Z_1 X_2 Z_3)$. $T'(\theta)$ consists solely of identities and Pauli-X operators, and so each part of $T'(\theta)$ commutes with $Z_1 X_2 Z_3$, with the exception of the X_1, X_3 terms (which obtain a negative sign under swapping the order). Therefore we have:

$$T'(\theta) Z_1 X_2 Z_3 = Z_1 X_2 Z_3 T''(\theta)$$

where:

$$T''(\theta) = (\cos\theta I_1 - \sin\theta X_1) \otimes (\cos\theta I_2 + \sin\theta X_2) \otimes (\cos\theta I_3 - \sin\theta X_3) \otimes \bigotimes_{i=4}^{2n} (\cos\theta I_i + \sin\theta X_i).$$

Hence we have:

$$\mathrm{Tr}(\rho_\theta Z_1 X_2 Z_3) = \mathrm{Tr}(T'(\theta)\rho_C T'(\theta) Z_1 X_2 Z_3) = \mathrm{Tr}(T'(\theta)\rho_C Z_1 X_2 Z_3 T''(\theta)) = \mathrm{Tr}(T''(\theta)T'(\theta)\rho_C)$$

where in the last equality we use that $Z_1 X_2 Z_3$ is a cluster state stabilizer (and hence can be absorbed into ρ_C), as well as the cyclicity of the trace. Computing $T''(\theta)T'(\theta)$, we find:

$$T''(\theta)T'(\theta) = (\cos^2\theta - \sin^2\theta) I_1 \otimes (I_2 + xX_2) \otimes (\cos^2\theta - \sin^2\theta) I_3 \otimes \bigotimes_{i=4}^{2n} (I_i + xX_i).$$

which using that $(\cos^2\theta - \sin^2\theta) = 1 - 4\sin^2\theta\cos^2\theta = 1 - x^2$, we can write as:

$$T''(\theta)T'(\theta) = \left(1 - x^2\right) \left(I_1 \otimes (I_2 + xX_2) \otimes I_3 \otimes \bigotimes_{i=4}^{2n} (I_i + xX_i) \right).$$

As before, only terms without Pauli-Zs in ρ_C will contribute to the trace (as there are no Pauli-Zs in $T''(\theta)T'(\theta)$ to cancel them out), which are again $\bigotimes_{i=1}^n I_i$, $\bigotimes_{i=1}^n X_i$, $I_1 X_2 \ldots I_{2n-1} X_{2n}$, and $X_1 I_2 \ldots X_{2n-1} I_{2n}$. When multiplying by $T''(\theta)T'(\theta)$, each of these contributes:

$$\begin{aligned}
\mathrm{Tr}(T''(\theta)T'(\theta) \bigotimes_{i=1}^{n} I_i) &= (1-x^2)2^{2n} \\
\mathrm{Tr}(T''(\theta)T'(\theta) I_1 X_2 \ldots I_{2n-1} X_{2n}) &= (1-x^2)2^{2n} x^n \\
\mathrm{Tr}(T''(\theta)T'(\theta) \bigotimes_{i=1}^{n} X_i) &= \mathrm{Tr}(T''(\theta)T'(\theta) X_1 I_2 \ldots X_{2n-1} I_{2n}) = 0
\end{aligned}$$

Where we note for the last equality that the two terms are traceless since $T''(\theta)T'(\theta)$ contains no X_1 or X_3 terms. We therefore have:

$$\mathrm{Tr}(\rho_\theta X_1) = \mathrm{Tr}\left(T''(\theta)T'(\theta) \left(\frac{1}{2^{2n}} \sum_{g \in S} \right) \right) = (1-x^2) + (1-x^2)x^n = (1-x^2)(1+x^n). \tag{A.8}$$

Combining equations (A.4), (A.6) and (A.7), we find:

$$\langle X_i \rangle_\theta = \frac{x(1+x^{n-2})(1+x^n)}{(1+x^n)^2} = \frac{x(1+x^{n-2})}{1+x^n}. \tag{A.9}$$

Additionally, combining equations (A.5), (A.6), and (A.8), we find:

$$\langle K_i \rangle_\theta = \frac{(1-x^2)(1+x^n)}{(1+x^n)^2} = \frac{1-x^2}{1+x^n}. \tag{A.10}$$

Equations (4.3) and (4.7) in the main body of the thesis are then just the $n = 2$ (ring of size $N = 4$) cases of the general expressions above.